Abbreviations and Acronyms

AP	= action potential
APD	= action potential duration
APD_{50}	= action potential duration measured at 50% repolarization
BCL	= basic cycle length
Brugada-ECG	= coved-type ST-segment elevation
Delta-Epi interval	= interval from the earliest to the latest epicardial activation
DR	= dispersion of repolarization
ECG	= electrocardiogram/electrocardiography
GR_{max}	= maximum gradient of repolarization
I_{Ca}	= inward calcium current
$I_{K\text{-}ATP}$	= ATP-sensitive potassium current
I_{Na}	= sodium current
I_{to}	= transient outward potassium current
P2R	= phase 2 re-entrant/entry
RV	= right ventricle/ventricular
Sti-Epi interval	= interval from the stimulus to the earliest epicardial activation
VF	= ventricular fibrillation
VT	= ventricular tachycardia

ization abnormalities interact and contribute to the development and maintenance of VF in the Brugada syndrome.

To investigate the heterogeneities of cellular repolarization and depolarization and their potential role in the development of re-entrant arrhythmias, we used a technique of high-resolution optical mapping, which allowed us to measure the electrical heterogeneity of APs on the epicardial or endocardial surface (18). We demonstrated that a steep repolarization gradient in the RV epicardium but not in the endocardium plays a key role in initiating P2R. Moreover, further depolarization and repolarization abnormalities degenerate the P2R-induced spiral re-entry into multiple wavelets forming VF in an experimental model of the Brugada syndrome.

METHODS

Canine RV wedge model of the Brugada syndrome. All animal care procedures were in accordance with the position of the American Heart Association research animal use (November 11, 1984). The methods used for isolation, perfusion, and recording of transmembrane activity from the arterially perfused canine RV (anterior wall) is similar to methods reported with canine wedge preparations (8,9). Briefly, a transmural wedge with dimensions of approximately 2 × 1 × 0.7 cm to 3 × 1.5 × 1 cm was dissected from the free wall of the RV of male dogs (n = 20), cannulated via the branch of right coronary artery, and placed in a small tissue bath. These preparations were arterially perfused between 40 and 60 mm Hg with Tyrode's solution (35 ± 1°C). The inward calcium current (I_{Ca}) and sodium current (I_{Na}) block with terfenadine (5 μmol/l), combined with augmentation of ATP-sensitive potassium current ($I_{K\text{-}ATP}$) with pinacidil (2 μmol/l), and I_{Na} block with pilsicainide (5 μmol/l) were used to create an experimental model of the Brugada syndrome (8–10,19).

After changing ECG to the coved-type ST-segment elevation mimicking the Brugada syndrome (Brugada-ECG) by administration of these drugs, 1) we recorded the spontaneous occurrence of closely coupled extrasystoles and subsequent non-sustained polymorphic VT (terminated within 5 s) or VF (sustained more than 5 s) during pacing from the endocardium at basic cycle length (BCL) of 2,000 ms (n = 10), and 2) we analyzed restitutions of the epicardial conduction velocity and action potential variable with a single extra stimulus (S2) delivered after every 10th basic beat (S1) paced from the epicardial surface at BCL of 1,000 ms (n = 10).

Transmembrane AP and ECG recording. A transmural ECG was recorded with Ag-AgCl electrodes, which were placed in the Tyrode's solution bathing the preparation, 1.0 cm from the epicardial and endocardial surfaces (epicardial, positive pole). The epicardial and endocardial APs were simultaneously recorded from the epicardial and endocardial surfaces with separate intracellular floating microelectrodes (direct current resistance 10 to 20 MΩ; 2.7 mmol/l potassium chloride) at positions approximating the transmural axis of the ECG.

Optical AP recording. After staining with the voltage sensitive dye, di-4-ANEPPS (5 μmol/l for 30 min), wedges were stabilized against a flat imaging window. Excitation of the dye's fluorescence was achieved with 480 ± 15 nm light through a bandpass filter (ANDV8247, Andover, Salem, New Hampshire) from a bluish-green emission diode (E1L51-3B0A4-02, Toyoda Gosei, Aichi, Japan). Fluoresced light from the wedge was split by a dichrotic mirror and narrowed down to the two frequency bands (approximately 540 or 690 nm) through a bandpass filter (ANDV8368 or ANDV7845, respectively, Andover). Then, the dual-wavelength lights were simultaneously focused onto 10-bit 256 × 256 element dual complementary metal oxide semiconductor (C-MOS) censors (Hamamatsu Photonics, Hamamatsu, Japan) with image intensifiers (FASTCAM-Ultima, Photron, Tokyo, Japan) at a 500 frames/s (Fig. 1).

Both optical signals were digitized at 0.5 kHz, and other amplified signals were digitized at 2 kHz with a 12-bit analog-to-digital converter, stored on the hard disk of a dedicated laboratory computer system, and analyzed with the original software of our laboratory. Therefore, after ratiometry of both signals to subtract a motion artifact, the voltage of the optical signal recorded at each site was automatically displayed in color (lowest, black; greatest, red) and plotted in the 256 × 256 matrix as an isopotential map, and transmembrane APs from 256 sites (16 × 16 units) on the RV epicardial or endocardial surface were displayed in control and in the Brugada-ECG condition with or without arrhythmic events. Moreover, phase analysis was used to display the pattern of wave propagation and wave-break during ventricular tachyarrhythmias (20,21).

Data analysis. Optical action potential duration (APD) was automatically measured at 50% repolarization (APD_{50}),

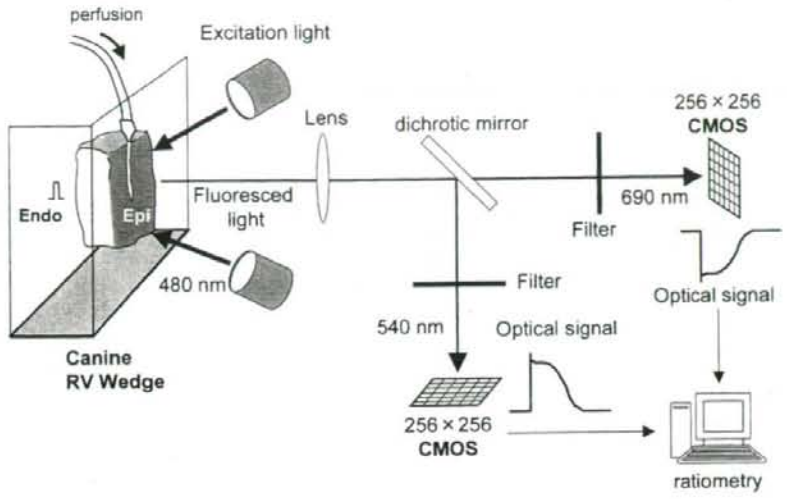

Figure 1. Schematic diagram showing the major components of high-resolution optical mapping of the epicardial (Epi) or endocardial (Endo) surface in an arterially perfused canine right ventricular (RV) wedge preparation. CMOS = complementary metal oxide semiconductor.

and the distributions of epicardial and endocardial APD_{50} were displayed as a repolarization counter map in baseline (control condition) and after changing to the Brugada-ECG with or without P2R-extrasystoles. The epicardial and endocardial DR were calculated from the maximum difference of repolarization times (activation time + APD) in the epicardial and endocardial surfaces, respectively. Transmural DR was calculated from the maximum difference between the epicardial and endocardial repolarization times recorded from the floating microelectrodes. Moreover, the maximum gradient of repolarization (GR_{max} = maximum Delta-APD_{50}/Delta-distance) in the epicardium and endocardium were calculated in each condition. We also measured depolarization parameters such as the interval from the stimulus to the earliest epicardial activation (Sti-Epi interval) and the interval from the earliest to the latest epicardial activation (Delta-Epi interval) during pacing from the endocardium in control and in the Brugada-ECG

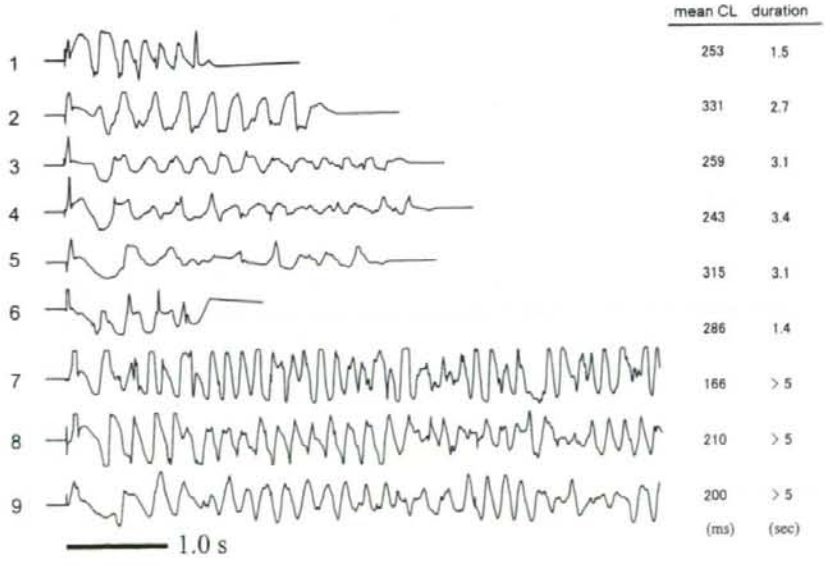

Figure 2. Representative episodes of polymorphic ventricular tachycardia or ventricular fibrillation (VF) in a canine wedge model of the Brugada syndrome. All arrhythmias were spontaneously developed after the electrocardiogram with coved-type ST-segment elevation. Many of the arrhythmias **(numbers 1 to 6)** terminated within a few seconds, but the others **(numbers 7 to 9)** with a shorter cycle length (CL) degenerated into VF, which continued more than 5 s.

condition. Conduction velocity (θ) was determined by linear regression of the isochrone distance versus activation time. Lines parallel and perpendicular to the fiber orientation were defined as the direction of longitudinal (L) and transverse (T) propagation, respectively. The optical data at edge of the preparation, with apparent contraction artifact, and noise level more than 20% of AP amplitude were excluded.

Statistical analysis. Statistical analysis of the data was performed with a Student's t test for paired data or analysis of variance coupled with Scheffe's test, as appropriate. Data is expressed as mean ± SD or mean ± SEM. Significance was defined as a value of $p < 0.05$.

RESULTS

Canine wedge model of the Brugada syndrome. Terfenadine combined with pinacidil and pilsicainide produced the Brugada-ECG in all preparations. There was no arrhythmia in control conditions, whereas combination of the drugs spontaneously developed a P2R-induced short-coupled extrasystole and subsequent polymorphic VT or VF in 9 of 10 preparations (Fig. 2). The QRS interval, QT interval, and J-point level in the ECG were significantly greater in the Brugada-ECG than in the control condition, but those parameters in the Brugada-ECG were not significantly different between beats with and without P2R-extrasystoles (Table 1).

Epicardial repolarization abnormality develops P2R-extrasystoles. Figure 3 represents the epicardial and endocardial APD_{50} contour map and optical APs in the control and in the Brugada-ECG condition with or without P2R-extrasystoles. In the control condition, the epicardial and endocardial APs were almost homogeneous (Figs. 3A and 3D). In contrast, in the Brugada-ECG, the AP morphology in the epicardium but not endocardium changed into heterogeneous, owing to a combination of abbreviated (loss-of-dome) and prolonged (restore-of-dome) APs, resulting in increasing DR in the epicardium rather than in the endocardium (Figs. 3B and 3E). Moreover, further prolonged AP at some areas in the epicardium was closely adjacent to the loss-of-dome APs (arrow), thus producing a repolarization mismatch within a small area and developing a P2R-extrasystole at the loss-of-dome site (Fig. 3C). The APs in the endocardium, however, were less heterogeneous than those in the epicardium even in the Brugada-ECG just before P2R-extrasystoles (Fig. 3F).

The composite data of repolarization and depolarization parameters in the control and in the Brugada-ECG condition with and without P2R-extrasystoles are shown in Table 1. In the Brugada-ECG, the epicardial maximum APD_{50} was significantly prolonged, whereas the epicardial minimum APD_{50} was significantly abbreviated compared with those in the control condition, thus significantly increasing the epicardial DR and GR_{max}. Moreover, the

Table 1. ECG, Repolarization, and Depolarization Parameters in Control and in the Brugada-ECG Condition With or Without Phase 2 Re-Entrant Extrasystoles

	Control	Brugada-ECG	
		P2R-PVC (−)	P2R-PVC (+)
ECG			
QRS duration (ms)	35 ± 4	63 ± 20*	66 ± 22*
QT interval (ms)	286 ± 30	335 ± 33*	—
J-point (mV)	0.04 ± 0.04	0.23 ± 0.08*	0.27 ± 0.08*
Repolarization			
Epicardium			
Max APD_{50} (ms)	239 ± 19	325 ± 86*	480 ± 92*†
Min APD_{50} (ms)	192 ± 16	100 ± 32*	89 ± 28*
Mean APD_{50} (ms)	214 ± 18	200 ± 62	244 ± 68†
DR (ms)	47 ± 11	228 ± 78*	383 ± 93*†
GR_{max} (ms/mm)	5 ± 5	46 ± 29*	176 ± 54*†
Endocardium			
Max APD_{50} (ms)	269 ± 23	269 ± 61	314 ± 77
Min APD_{50} (ms)	214 ± 28	171 ± 53	183 ± 55
Mean APD_{50} (ms)	244 ± 27	219 ± 63	258 ± 70
DR (ms)	56 ± 13	98 ± 44	123 ± 41*
GR_{max} (ms/mm)	8 ± 4	20 ± 13	26 ± 10*
Transmural			
DR (ms)	28 ± 8	135 ± 36*	131 ± 41*
Depolarization			
Sti-Epi interval (ms)	26 ± 10	46 ± 9*	47 ± 12*
Delta-Epi interval (ms)	12 ± 4	19 ± 18	24 ± 20

Values are mean ± SD. *$p < 0.05$ versus control; †$p < 0.05$ versus coved-type ST-segment elevation (Brugada-ECG) condition without P2R-PVC by analysis of variance with Scheffe's test.

APD_{50} = action potential duration at 50% repolarization; Delta-Epi = interval from the earliest to the latest epicardial activation; DR = dispersion of repolarization; GR_{max} = maximum gradient of repolarization; Max = maximum; Min = minimum; P2R-PVC = phase 2 re-entrant extrasystoles; Sti-Epi = interval from the stimulus to the epicardium.

JACC Vol. 47, No. 10, 2006
May 16, 2006:2074–85

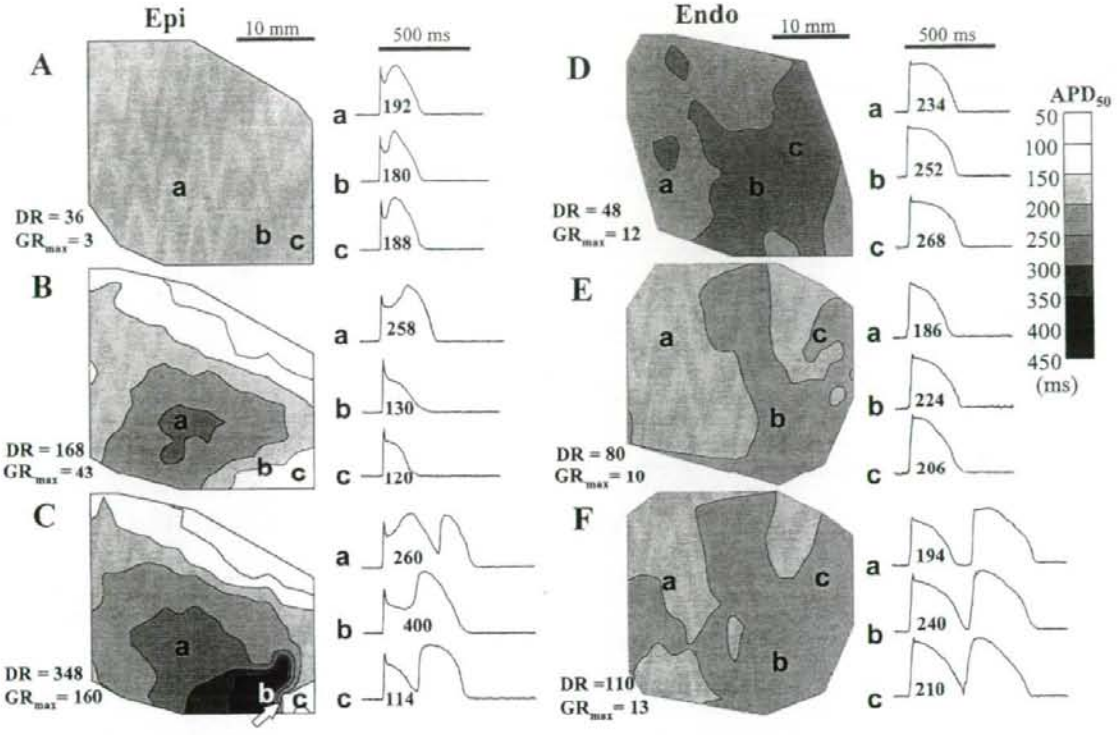

Figure 3. Representative action potential duration measured at 50% repolarization (APD_{50}) contour map on the right ventricular epicardium (Epi) and endocardium (Endo) in control condition (**A and D**, respectively), in the ST-segment elevation (Brugada-ECG) without phase 2 re-entrant (P2R) extrasystoles (**B and E**, respectively), and in the Brugada-ECG just before P2R extrasystoles (**C and F**, respectively) and representative optical action potentials at each site (**a to c**). **White arrow** = initial site of P2R. DR = dispersion of repolarization; GR_{max} = maximum gradient of repolarization.

epicardial maximum APD_{50} was further prolonged in the Brugada-ECG just before P2R-extrasystoles compared with that without P2R-extrasystoles, thus remarkably increasing the epicardial DR and GR_{max}. The endocardial repolarization parameters, however, were not significantly changed after the Brugada-ECG. Moreover, there was no significant difference in the endocardial repolarization parameters between the Brugada-ECG with and without P2R-extrasystoles. Owing to a different response of APD between the epicardium and endocardium, transmural DR was significantly increased in the Brugada-ECG compared with that in the control condition but was not significantly different between the Brugada-ECG condition with and without P2R-extrasystoles.

Regarding depolarization parameters, the Sti-Epi interval was significantly increased in the Brugada-ECG compared with in the control condition but was not different between the condition with and without P2R-extrasystoles. The Delta-Epi interval was not significantly different among the three conditions.

Threshold to develop P2R-extrasystoles. A total of 41 episodes of spontaneous P2R-extrasystoles after the Brugada-ECG were successfully mapped in 9 of 10 preparations, and 33 (80%) of them were originated from the GR_{max} area in the epicardium. As shown in Figure 4, the epicardial GR_{max} was significantly greater in the Brugada-ECG than in control condition. The GR_{max} of 99 ms/mm (dashed line) showed that P2R-extrasystoles were spontaneously developed in the Brugada-ECG. In contrast, the endocardial GR_{max} and transmural DR were greater in the Brugada-ECG condition compared with the control condition but were not different between the Brugada-ECG condition with and without P2R-extrasystoles.

Figure 5A shows the epicardial isopotential map representing the distribution of loss-of-dome and restore-of-dome area in the Brugada-ECG with (beat 2) or without (beat 1) a P2R-extrasystole. Figures 5B and 5C show the depolarization map during the P2R-extrasystole and optical APs at each site on the epicardial surface. At the timing of phase 2 (120 to 190 ms), the restore-of-dome area (orange-red) was larger in the beat 2 than in the beat 1. Moreover, the larger AP dome in the beat 2 moved from a restore-of-dome site (site a and b) to a nearby loss-of-dome site (site d), producing re-excitation at the loss-of-dome site and propagating in a counterclockwise fashion around the refractory region of the epicardium.

P2R-extrasystoles induce polymorphic VT or VF. The epicardial P2R-extrasystoles produced 12 episodes of self-

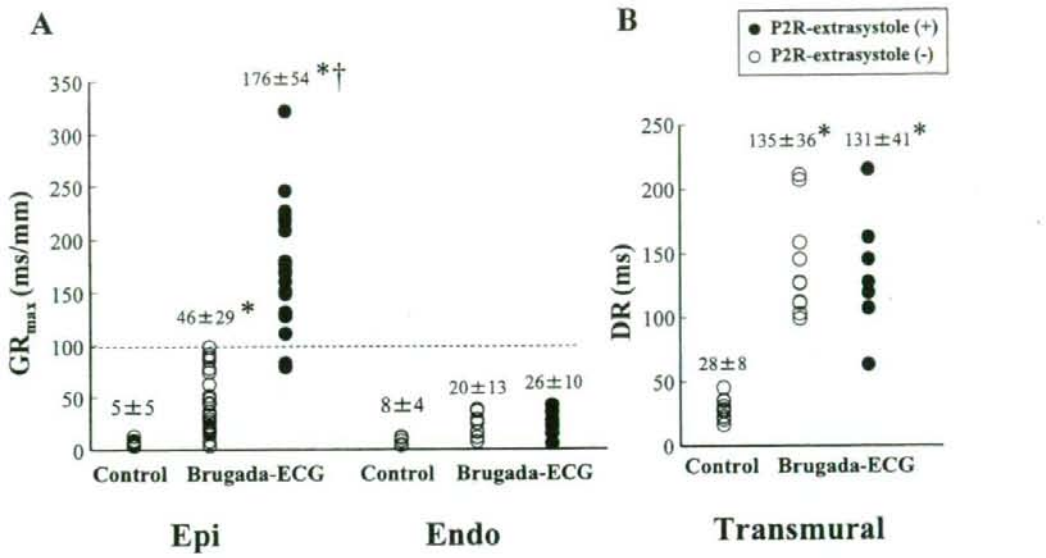

Figure 4. Scatter plots of the maximum gradient of repolarization (GR_{max}) in the epicardial (Epi) and endocardial (Endo) surfaces **(A)** and transmural dispersion of repolarization (DR) **(B)** in control and the ST-segment elevation (Brugada-ECG) condition with **(closed circles)** or without **(open circles)** phase 2 re-entrant (P2R) extrasystoles. Values are mean ± SD. *p < 0.05 versus control condition; †p < 0.05 versus Brugada-ECG condition without P2R-extrasystole by analysis of variance with Scheffe's test.

terminating (<5 s) polymorphic VT and 5 episodes of sustained (≥5 s) VF. The mechanism underlying the difference between the polymorphic VT and VF is shown in representative examples in Figures 6 and 7. The epicardial GR_{max} area (arrow) developed P2R-extrasystole in both cases (Figs. 6A and 7A); however, the epicardial depolarization map paced from the endocardium at BCL of 2,000 ms shows a remarkable conduction delay in the episode of VF (Fig. 7B) compared with that of polymorphic VT (Fig. 6B). We compared the repolarization and depolarization parameters just before the P2R-induced polymorphic VT and VF in Table 2. There was no significant difference in the repolarization parameters between the two groups; however, the depolarization parameters such as QRS, Sti-Epi, and Delta-Epi intervals were significantly longer in the VF group than in the polymorphic VT group.

Figures 6C and 6D represent phase map and optical APs, respectively, during the P2R-induced polymorphic VT, showing that re-entry was initiated from the epicardial GR_{max} area and rotated mainly in the epicardium without wave-break. In contrast, Figures 7C and 7D represent those during the P2R-induced VF, showing that the development of initial P2R was similar to that of polymorphic VT, but the first P2R-wave was broken up into the multiple wavelets, resulting in degenerating VT into VF. The phase singularity points during the first P2R-wave almost coincided with the sites of delayed conduction (Fig. 7B). In all VF cases, the wave was broken up into multiple wandering wavelets during the first P2R-induced extrasystole; however, in the polymorphic VT cases, only 3 of 12 (25%) cases had a wave-break after the second beat, but soon after the wave had been broken, the waves collided and finally terminated.

Conduction and APD restitutions by S1-S2 method. In another 10 preparations, we analyzed the epicardial conduction velocity and APD restitutions to show the mechanisms underlying the wave-break during the first re-entrant wave in the VF cases. The epicardial longitudinal and transverse conduction velocities (θ_L and θ_T) in the VF cases (n = 5) were significantly slower than those in the polymorphic VT cases (n = 5) under the Brugada-ECG condition, and the conduction velocity restitution curve in the VF cases was shifted lower in parallel (Fig. 8).

In contrast, the epicardial APD was abbreviated and its restitution was flat in the polymorphic VT case under the Brugada-ECG condition, owing to loss of AP dome (Fig. 9B); however, in the VF case, shorter S1-S2 interval (≤300 ms) rather prolonged APD because of restoration of AP dome. Moreover, this restoration was heterogeneous in the epicardial surface, increasing the epicardial DR (Fig. 9C). This "inverse" APD restitution pattern was observed in four of five VF cases but in only one of five polymorphic VT cases under the Brugada-ECG condition.

DISCUSSION

Repolarization mismatch develops P2R-extrasystoles. All-or-none repolarization of the ventricular AP and P2R is considered to be one of the potential mechanism of the ST-segment elevation and subsequent VF in the Brugada

JACC Vol. 47, No. 10, 2006
May 16, 2006:2074–85

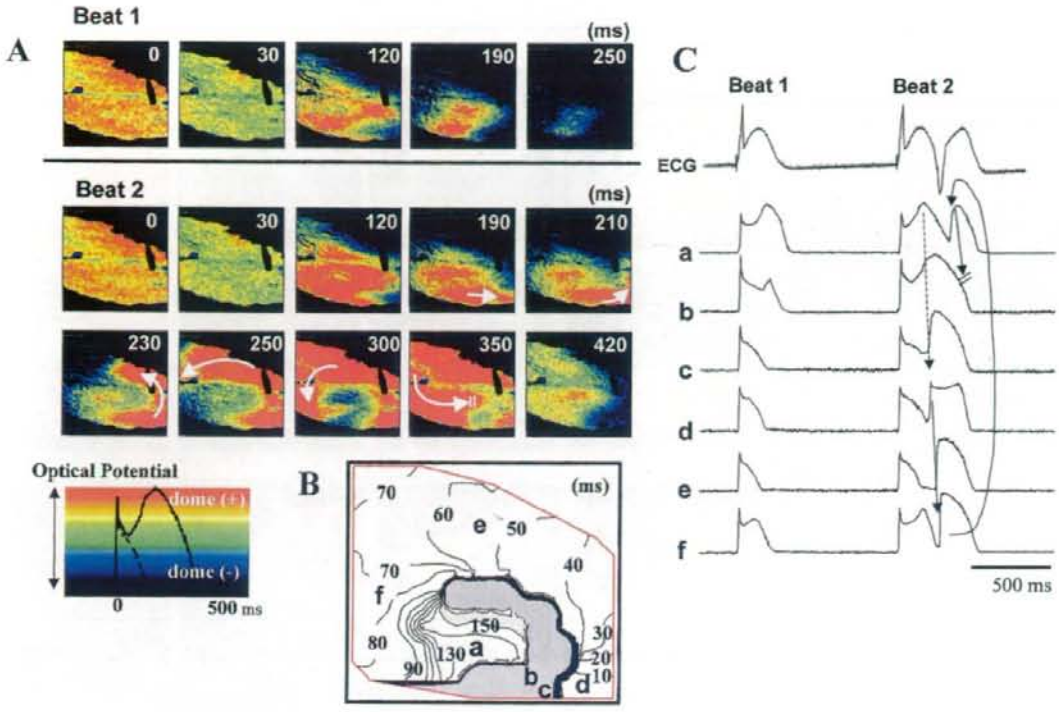

Figure 5. Snapshots of a color optical isopotential movie on the epicardial surface for the continuous two beats with (Beat 2) and without (Beat 1) a phase 2 re-entrant extrasystole (P2R-extrasystole) in the Brugada-ECG condition **(A)**. Depolarization map of a P2R-extrasystole **(B)** and optical action potentials at each site **(a to f)** and transmural electrocardiogram (ECG) **(C)**. Please see the Appendix for accompanying video.

syndrome (7–9,12); however, because of limitations of conventional electrophysiological recording techniques, it remains unknown to what extent the heterogeneity of APs is required for developing P2R-extrasystoles in the Brugada-ECG. In this study, we conducted a high-resolution optical mapping in canine RV wedge preparation, which allowed a detailed measurement of cellular repolarization and depolarization in the epicardial and endocardial surfaces. First, we photographed the moment that P2R-extrasystoles in the Brugada-ECG occurred and produced re-entrant arrhythmias such as polymorphic VT or VF. A unique topographical distribution of both loss-of-dome and restore-of-dome cells in the epicardium but not endocardium might underlie a key feature of the Brugada phenotype, including coved-type ST-segment elevation and susceptibility to P2R-induced ventricular tachyarrhythmias. It must be essential to develop P2R-extrasystoles that further prolong the epicardial AP results in loss-of-dome at some areas but not at the closely adjacent area, making a steep repolarization mismatch. These data are consistent with some clinical reports that the QT interval is more prolonged in the right precordial leads than in other leads during typical coved-type Brugada-ECG (2,13,22) and that VF in the Brugada syndrome was frequently induced by the specific premature ventricular contractions originated from the free wall of RV outflow tract (23,24).

Ionic backgrounds of Brugada-ECG and P2R-extrasystoles. Previous experimental studies pharmacologically created the Brugada-ECG by using various drugs and/or conditions capable of causing an outward shift in the current active at the end of phase 1 of RV epicardium (e.g., increase in I_{to}, $I_{K\text{-}ATP}$, and/or $I_{K\text{-}ACh}$ and decrease in I_{Ca} and I_{Na}) (4,7–10,19). Moreover, a development of P2R on the basis of the all-or-none repolarization phenomenon might depend on a fine balance of I_{to}, I_{Na}, and I_{Ca}. We used block of I_{Ca} and I_{Na} (and other currents) with terfenadine (5 μmol/l), combined with augmentation of $I_{K\text{-}ATP}$ with pinacidil (2 μmol/l) and I_{Na} block with pilsicainide (5 μmol/l); a combination that is most likely to produce the Brugada-ECG. The reason a loss-of-dome occurred in some areas but not others in the epicardium is expected to be owing to an intrinsic difference in I_{to} (25). Miyoshi et al. (26) investigated the mechanism of P2R by their mathematical model and suggested that P2R was developed from a boundary area (0.8 cm) between loss-of-dome and restore-of-dome where a fine balance between I_{to} and $I_{Ca,L}$ was required and that $I_{Ca,L}$ must play an essential role in the genesis of P2R. This mathematical model

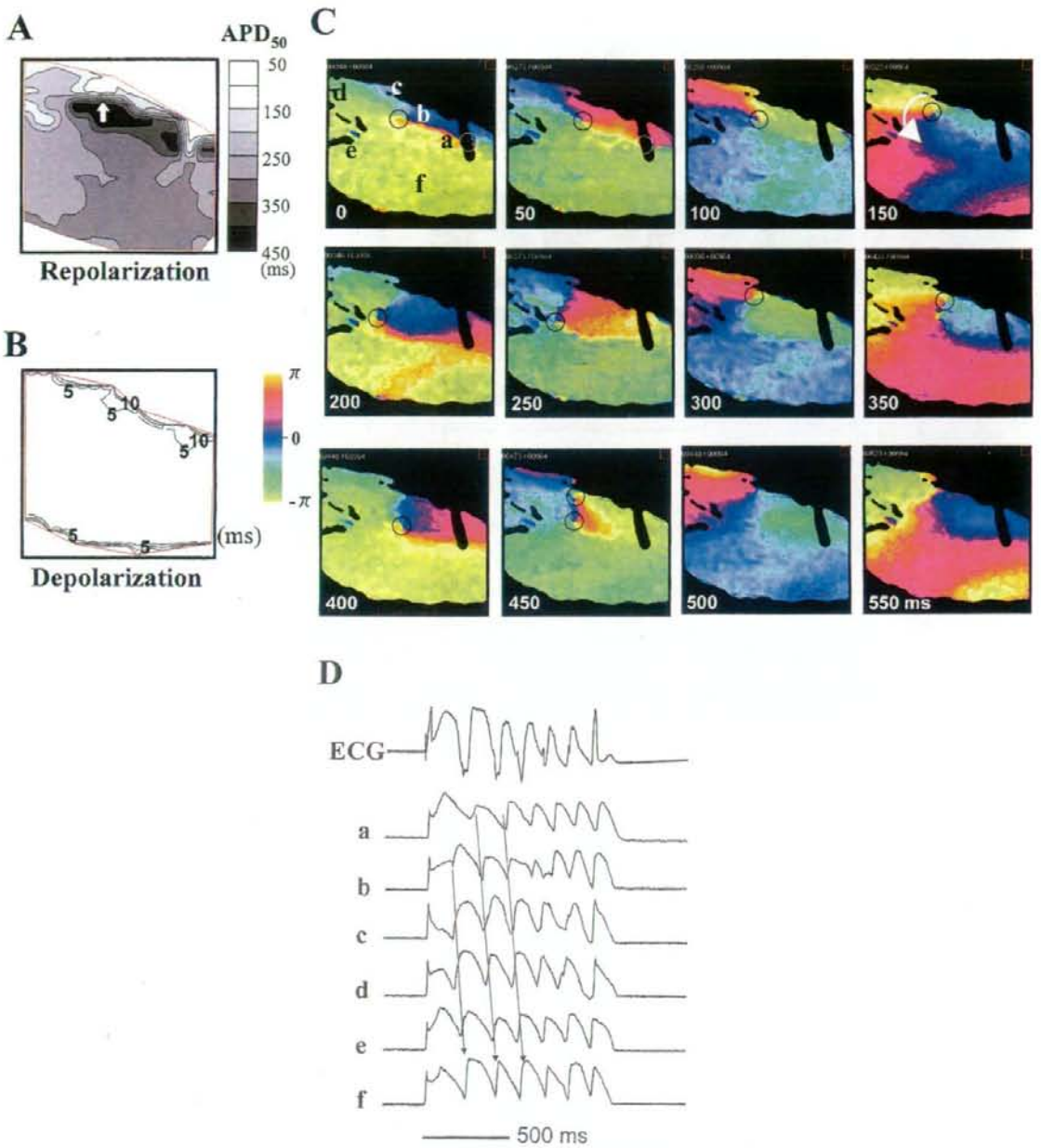

Figure 6. Representative repolarization and depolarization maps on the epicardial surface in the ST-segment elevation (Brugada-ECG) condition just before non-sustained polymorphic ventricular tachycardia (VT) (**A, B**), snapshots of phase movie during polymorphic VT originated from the epicardial phase 2 re-entry (**C**), and optical action potentials at each site (**a to f**) together with a transmural electrocardiogram (ECG) (**D**). **Open circles** = singularity points. APD_{50} = action potential duration at 50% repolarization. Please see the Appendix for accompanying video.

JACC Vol. 47, No. 10, 2006
May 16, 2006:2074–85

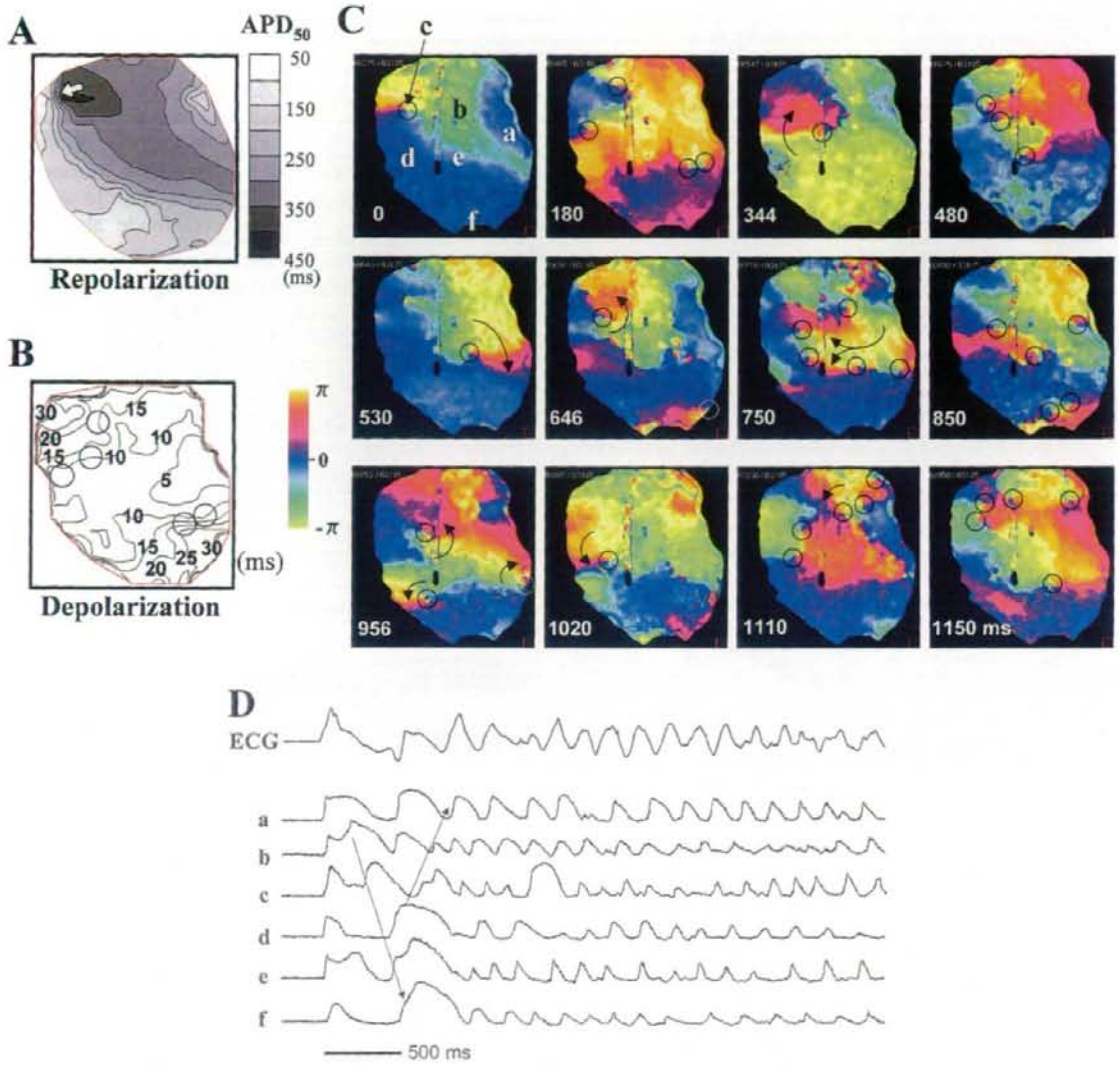

Figure 7. Representative repolarization and depolarization maps on the epicardial surface in the ST-segment elevation (Brugada-ECG) condition just before ventricular fibrillation (VF) **(A, B)**, snapshots of phase movie during VF originated from the epicardial phase 2 re-entry **(C)**, and optical action potentials at each site **(a to f)** together with a transmural electrocardiogram (ECG) **(D)**. **Open circles** = singularity points. APD_{50} = action potential duration at 50% repolarization. Please see the Appendix for accompanying videos.

supports our data that most of P2R-extrasystoles were developed from a small area (<0.5 cm) of GR_{max}.

Maintenance of VF. The only gene linked to the Brugada syndrome is cardiac sodium channel gene, *SCN5A* (17,27). Moreover, sodium channel blockades often unmask Brugada-phenotype, because a loss of sodium channels function enhances both repolarization and depolarization abnormalities (25,28,29). Our experimental study used a pure sodium channel blocker, pilsicainide, to produce the Brugada-ECG associated with prolonged QRS duration and conduction parameters; however, in the Brugada-ECG condition, the depolarization parameters were not different in beats with and without P2R-extrasystoles. In contrast, slower conduction was closely associated with VF susceptibility. These findings suggest that depolarization disturbance was not directly associated with the development of P2R-extrasystole, a trigger of VF, but might contribute to the maintenance of VF in the Brugada-ECG condition.

Electrophysiologic mechanism of VF in the Brugada syndrome has been considered to be re-entry because of high inducibility and reproducibility of VT/VF by pro-

Table 2. ECG, Optical Repolarization, and Depolarization Parameters Just Before Polymorphic VT or VF in the Brugada-ECG Condition

	PVT (n = 12)	VF (n = 5)	p Value
VT/VF CL (ms)	325 ± 33	190 ± 23	<0.001
QRS duration (ms)	74 ± 18	102 ± 23	0.009
J-point (mV)	0.48 ± 0.31	0.43 ± 0.15	NS
Epi max-min APD_{50} (ms)	394 ± 79	344 ± 88	NS
Epi GR_{max} (ms/mm)	169 ± 55	157 ± 22	NS
Sti-Epi interval (ms)	43 ± 10	60 ± 16	0.03
Delta-Epi interval (ms)	13 ± 3	41 ± 16	0.001

Values are mean ± SD.
CL = averaged tachycardia cycle length; PVT = polymorphic ventricular tachycardia; VF = ventricular fibrillation; VT = ventricular tachycardia; other abbreviations as in Table 1.

grammed electrophysiologic stimulation (3,6,14,30), although it is still unclear how VF re-entry is maintained in the Brugada syndrome. In this study, most of the polymorphic VT was single or figure-of-eight type re-entry with no wave-break and terminated within a few seconds (Fig. 6C). In contrast, wave-break in VF group occurred during the first re-entrant wave and took place at sites of the delayed epicardial conduction (Fig. 7B). Wu et al. (31) demonstrated that Ca^{2+} and fast Na^+ current inhibition turned fast VF into slow VF by flattering APD restitution and increasing conduction time. In this Brugada model, however, VF was characterized as the shorter cycle length and multiple wandering wavelets (Fig. 7C) in spite of the slower conduction (Fig. 8), because APD restitution was not flat but rather an "inverse" pattern (Fig. 9), thus increasing dispersion of repolarization during tachycardia. Krishnan and Antzelevitch (25) had demonstrated the incremental arrhythmogenesis of Na^+ channel dysfunction in the RV epicardium during tachycardia. Flecainide also rate-dependently slowed down the conduction velocity. Thus, fast Na^+ current inhibition strongly enhances both heterogeneity of repolarization and conduction slowing during tachycardia in the Brugada-ECG model, which can easily break up the spiral re-entry, thus degenerating polymorphic VT into VF with multiple wavelets.

Clinical implication. Previous clinical study suggested that induction of VF by programmed ventricular stimulation depended on the severity of depolarization abnormalities such as a longer QRS duration or His-ventricular interval but did not predict the recurrence of cardiac events in symptomatic Brugada syndrome (14,15). Moreover, depolarization and repolarization abnormalities in this syndrome are now considered to be closely correlated (16,29,32,33), supporting our data that both repolarization and depolar-

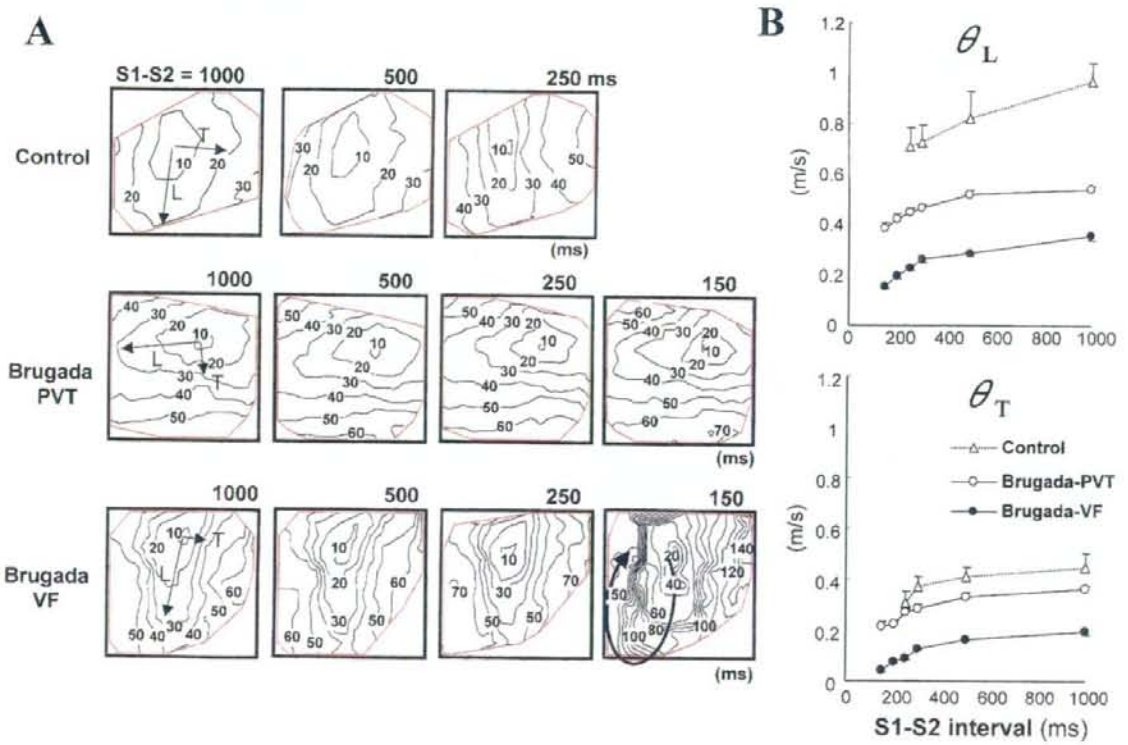

Figure 8. Representative epicardial depolarization maps paced from the epicardium by S1-S2 method in the control and ST-segment elevation (Brugada-ECG) condition with polymorphic ventricular tachycardia (PVT) or ventricular fibrillation (VF) **(A)**, and longitudinal (L) and transverse (T) conduction velocity (θ) restitution curves in each condition **(B)**. Values are mean ± SEM.

JACC Vol. 47, No. 10, 2006
May 16, 2006:2074–85

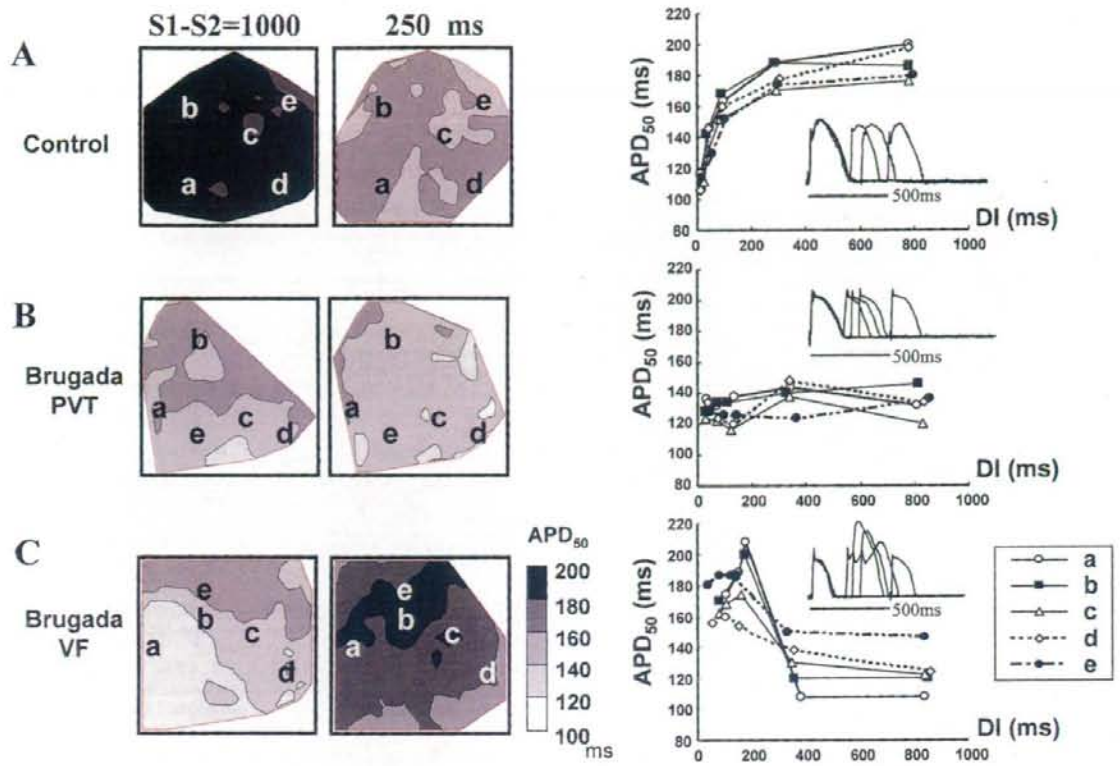

Figure 9. Representative epicardial repolarization maps paced from the epicardium by S1-S2 method and plot of the restitution of action potential duration at each site **(a to e)** and superimposed optical action potentials at site b in control condition **(A)**, and the Brugada-ECG condition with polymorphic ventricular tachycardia (PVT) **(B)** or ventricular fibrillation (VF) **(C)**. APD_{50} = action potential duration at 50% repolarization; DI = diastolic interval.

ization abnormalities were important in the development of VF. Our results, for the first time, revealed how repolarization and depolarization abnormalities interact in developing a trigger of premature ventricular complexes and in maintaining VF in the Brugada-ECG condition. A steep repolarization gradient in the epicardium introduced P2R-extrasystoles and subsequent non-sustained polymorphic VT, and further increased depolarization and repolarization abnormalities maintained VF, thus increasing risk of sudden cardiac death.

Study limitations. First, we mapped the epicardial or endocardial surface separately in each condition. Therefore, the two-dimensional mapping technique used in this study provides only limited insights into the number of spiral waves and these re-entrant patterns and could not directly evaluate the relationship between the transmural gradient of repolarization and arrhythmogenesis in the Brugada-ECG condition. A second limitation is the size of wedge preparation. It is unclear whether a polymorphic VT or VF in the wedges can result in those with larger hearts. Third, we pharmacologically created, similarly to the methods of previous studies, the Brugada-phenotype, which could not be a complete surrogate for the Brugada syndrome. Finally, with optical mapping, there is a major concern about motion artifacts that can greatly distort the AP recorded, but our ratio-metric methods can reduce motion artifacts without using an uncoupler.

Reprint requests and correspondence: Dr. Wataru Shimizu, Division of Cardiology, Department of Internal Medicine, National Cardiovascular Center, 5-7-1 Fujishiro-dai, Suita, Osaka, 565-8565 Japan. E-mail: wshimizu@hsp.ncvc.go.jp.

REFERENCES

1. Brugada P, Brugada J. Right bundle branch block, persistent ST-segment elevation and sudden cardiac death: a distinct clinical and electrocardiographic syndrome. A multicenter report. J Am Coll Cardiol 1992;20:1391–6.
2. Wilde AA, Antzelevitch C, Borggrefe M, et al. Proposed diagnostic criteria for the Brugada syndrome: consensus report. Circulation 2002; 106:2514–9.
3. Brugada J, Brugada R, Antzelevitch C, Towbin J, Nademanee K, Brugada P. Long-term follow-up of individuals with the electrocardiographic pattern of right bundle-branch block and ST-segment elevation in precordial leads V1 to V3. Circulation 2002;105:73–8.
4. Antzelevitch C, Brugada P, Borggrefe M, et al. Brugada syndrome: report of the second consensus conference: endorsed by the Heart Rhythm Society and the European Heart Rhythm Association. Circulation 2005;111:659–70.
5. Brugada J, Brugada R, Brugada P. Determinants of sudden cardiac death in individuals with the electrocardiographic pattern of Brugada

syndrome and no previous cardiac arrest. Circulation 2003;108: 3092–6.
6. Priori SG, Napolitano C, Gasparini M, et al. Natural history of Brugada syndrome: insights for risk stratification and management. Circulation 2002;105:1342–7.
7. Antzelevitch C, Brugada P, Brugada J, Brugada R, Towbin JA, Nademanee K. Brugada syndrome: 1992–2002: a historical perspective. J Am Coll Cardiol 2003;41:1665–71.
8. Yan GX, Antzelevitch C. Cellular basis for the Brugada syndrome and other mechanisms of arrhythmogenesis associated with ST-segment elevation. Circulation 1999;100:1660–6.
9. Di Diego JM, Cordeiro JM, Goodrow RJ, et al. Ionic and cellular basis for the predominance of the Brugada syndrome phenotype in males. Circulation 2002;106:2004–11.
10. Fish JM, Antzelevitch C. Role of sodium and calcium channel block in unmasking the Brugada syndrome. Heart Rhythm 2004;1:210–7.
11. Kurita T, Shimizu W, Inagaki M, et al. The electrophysiologic mechanism of ST-segment elevation in Brugada syndrome. J Am Coll Cardiol 2002;40:330–4.
12. Lukas A, Antzelevitch C. Phase 2 re-entry as a mechanism of initiation of circus movement re-entry in canine epicardium exposed to simulated ischemia. Cardiovasc Res 1996;32:593–603.
13. Nademanee K, Veerakul G, Nimmannit S, et al. Arrhythmogenic marker for the sudden unexplained death syndrome in Thai men. Circulation 1997;96:2595–600.
14. Kanda M, Shimizu W, Matsuo K, et al. Electrophysiologic characteristics and implications of induced ventricular fibrillation in symptomatic patients with Brugada syndrome. J Am Coll Cardiol 2002;39: 1799–805.
15. Ikeda T, Sakurada H, Sakabe K, et al. Assessment of noninvasive markers in identifying patients at risk in the Brugada syndrome: insight into risk stratification. J Am Coll Cardiol 2001;37:1628–34.
16. Nagase S, Kusano KF, Morita H, et al. Epicardial electrogram of the right ventricular outflow tract in patients with the Brugada syndrome: using the epicardial lead. J Am Coll Cardiol 2002;39:1992–5.
17. Smits JP, Eckardt L, Probst V, et al. Genotype-phenotype relationship in Brugada syndrome: electrocardiographic features differentiate SCN5A-related patients from non-SCN5A-related patients. J Am Coll Cardiol 2002;40:350–6.
18. Akar FG, Spragg DD, Tunin RS, Kass DA, Tomaselli GF. Mechanisms underlying conduction slowing and arrhythmogenesis in nonischemic dilated cardiomyopathy. Circ Res 2004;95:717–25.
19. Kimura M, Kobayashi T, Owada S, et al. Mechanism of ST elevation and ventricular arrhythmias in an experimental Brugada syndrome model. Circulation 2004;109:125–31.
20. Gray RA, Pertsov AM, Jalife J. Spatial and temporal organization during cardiac fibrillation. Nature 1998;392:75–8.
21. Liu YB, Peter A, Lamp ST, Weiss JN, Chen PS, Lin SF. Spatiotemporal correlation between phase singularities and wavebreaks during ventricular fibrillation. J Cardiovasc Electrophysiol 2003;14:1103–9.
22. Pitzalis MV, Anaclerio M, Iacoviello M, et al. QT-interval prolongation in right precordial leads: an additional electrocardiographic hallmark of Brugada syndrome. J Am Coll Cardiol 2003;42:1632–7.
23. Kakishita M, Kurita T, Matsuo K, et al. Mode of onset of ventricular fibrillation in patients with Brugada syndrome detected by implantable cardioverter defibrillator therapy. J Am Coll Cardiol 2000;36: 1646–53.
24. Morita H, Fukushima-Kusano K, Nagase S, et al. Site-specific arrhythmogenesis in patients with Brugada syndrome. J Cardiovasc Electrophysiol 2003;14:373–9.
25. Krishnan SC, Antzelevitch C. Flecainide-induced arrhythmia in canine ventricular epicardium. Phase 2 re-entry? Circulation 1993;87: 562–72.
26. Miyoshi S, Mitamura H, Fujikura K, et al. A mathematical model of phase 2 re-entry: role of L-type Ca current. Am J Physiol Heart Circ Physiol 2003;284:H1285–94.
27. Chen Q, Kirsch GE, Zhang D, et al. Genetic basis and molecular mechanism for idiopathic ventricular fibrillation. Nature 1998;392: 293–6.
28. Brugada R, Brugada J, Antzelevitch C, et al. Sodium channel blockers identify risk for sudden death in patients with ST-segment elevation and right bundle branch block but structurally normal hearts. Circulation 2000;101:510–5.
29. Shimizu W, Antzelevitch C, Suyama K, et al. Effect of sodium channel blockers on ST segment, QRS duration, and corrected QT interval in patients with Brugada syndrome. J Cardiovasc Electrophysiol 2000; 11:1320–9.
30. Gasparini M, Priori SG, Mantica M, et al. Programmed electrical stimulation in Brugada syndrome: how reproducible are the results? J Cardiovasc Electrophysiol 2002;13:880–7.
31. Wu TJ, Lin SF, Weiss JN, Ting CT, Chen PS. Two types of ventricular fibrillation in isolated rabbit hearts: importance of excitability and action potential duration restitution. Circulation 2002;106: 1859–66.
32. Hisamatsu K, Kusano KF, Morita H, et al. Relationships between depolarization abnormality and repolarization abnormality in patients with Brugada syndrome. J Cardiovasc Electrophysiol 2004;15:870–6.
33. Tukkie R, Sogaard P, Vleugels J, de Groot IK, Wilde AA, Tan HL. Delay in right ventricular activation contributes to Brugada syndrome. Circulation 2004;109:1272–7.

APPENDIX

For accompanying videos to Figures 5, 6, and 7, please see the online version of this article.

Am J Physiol Heart Circ Physiol 291: H318–H326, 2006.
First published February 24, 2006; doi:10.1152/ajpheart.00975.2005.

Short-term electroacupuncture at Zusanli resets the arterial baroreflex neural arc toward lower sympathetic nerve activity

Daisaku Michikami,[1,2] Atsunori Kamiya,[1] Toru Kawada,[1] Masashi Inagaki,[1] Toshiaki Shishido,[1] Kenta Yamamoto,[1,2] Hideto Ariumi,[1,2] Satoshi Iwase,[3] Junichi Sugenoya,[3] Kenji Sunagawa,[4] and Masaru Sugimachi[1]

[1]*Department of Cardiovascular Dynamics, Advanced Medical Engineering Center, National Cardiovascular Center Research Institute, Osaka;* [2]*Pharmaceuticals and Medical Devices Agency, Tokyo;* [3]*Department of Physiology, School of Medicine Aichi Medical University, Nagakute, Aichi; and* [4]*Department of Cardiovascular Medicine, Kyushu University Graduate School of Medical Sciences, Fukuoka, Japan*

Submitted 12 September 2005; accepted in final form 17 February 2006

Michikami, Daisaku, Atsunori Kamiya, Toru Kawada, Masashi Inagaki, Toshiaki Shishido, Kenta Yamamoto, Hideto Ariumi, Satoshi Iwase, Junichi Sugenoya, Kenji Sunagawa, and Masaru Sugimachi. Short-term electroacupuncture at Zusanli resets the arterial baroreflex neural arc toward lower sympathetic nerve activity. *Am J Physiol Heart Circ Physiol* 291: H318–H326, 2006. First published February 24, 2006; doi:10.1152/ajpheart.00975.2005.—Although electroacupuncture reduces sympathetic nerve activity (SNA) and arterial pressure (AP), the effects of electroacupuncture on the arterial baroreflex remain to be systematically analyzed. We investigated the effects of electroacupuncture of Zusanli on the arterial baroreflex using an equilibrium diagram comprised of neural and peripheral arcs. In anesthetized, vagotomized, and aortic-denervated rabbits, we isolated carotid sinuses and changed intra-carotid sinus pressure (CSP) from 40 to 160 mmHg in increments of 20 mmHg/min while recording cardiac SNA and AP. Electroacupuncture of Zusanli was applied with a pulse duration of 5 ms and a frequency of 1 Hz. An electric current 10 times the minimal threshold current required for visible muscle twitches was used and was determined to be 4.8 ± 0.3 mA. Electroacupuncture for 8 min decreased SNA and AP ($n = 6$). It shifted the neural arc (i.e., CSP-SNA relationship) to lower SNA but did not affect the peripheral arc (i.e., SNA-AP relationship) ($n = 8$). SNA and AP at the closed-loop operating point, determined by the intersection of the neural and peripheral arcs, decreased from 100 ± 4 to 80 ± 9 arbitrary units and from 108 ± 9 to 99 ± 8 mmHg (each $P < 0.005$), respectively. Peroneal denervation eliminated the shift of neural arc by electroacupuncture ($n = 6$). Decreasing the pulse duration to <2.5 ms eliminated the effects of SNA and AP reduction. In conclusion, short-term electroacupuncture resets the neural arc to lower SNA, which moves the operating point toward lower AP and SNA under baroreflex closed-loop conditions.

arterial pressure; equilibrium diagram

ALTHOUGH THERE ARE MANY clinical case reports (21, 30, 32, 39, 40, 42), the effects of electroacupuncture on cardiovascular regulation remain to be systematically investigated. There has been a recent renewal of interest in the inhibitory effects of electroacupuncture of the Zusanli acupoint on the cardiovascular system, including reductions in arterial pressure (AP), heart rate, (3, 15, 16), and sympathetic nerve activity (SNA) (25, 42). Such inhibitory effects are observed during low-frequency (<20 Hz) electroacupuncture. Because the arterial baroreflex is one of the most important control systems that stabilize AP, we quantified the effects of electroacupuncture on the arterial baroreflex over an entire operating range. Systematic analysis would help to assess the possible utility of electroacupuncture as a treatment modality for certain cardiovascular diseases with vagolytic and sympathotonic states (26, 38).

One of the best ways to quantitatively analyze changes in the arterial baroreflex over an entire operating range may be analysis using a baroreflex equilibrium diagram (10, 23, 31) (see APPENDIX for details). Briefly, the baroreflex equilibrium diagram consists of a neural arc representing SNA as a function of baroreceptor input pressure and a peripheral arc representing AP as a function of SNA. The intersection of the two arcs corresponds to an operating point of the AP regulation under baroreflex closed-loop conditions. Considering the reduced AP and SNA found in previous studies, we hypothesized that short-term electroacupuncture resets the arterial baroreflex neural arc to lower SNA. In the present study, to test this hypothesis, we constructed a baroreflex equilibrium diagram with neural and peripheral arcs in anesthetized rabbits. The present findings indicate that electroacupuncture resets the baroreflex neural arc to lower SNA, moving the closed-loop operating point toward lower AP and SNA.

MATERIALS AND METHODS

Surgical Preparation

Animals were cared for in strict accordance with the *Guiding Principles for the Care and Use of Animals in the Field of Physiological Sciences* approved by the Physiological Society of Japan. Twenty-two Japanese White rabbits weighing 2.4–3.3 kg were anesthetized via intravenous injection (2 ml/kg) with a mixture of urethane (250 mg/ml) and α-chloralose (40 mg/ml) and mechanically ventilated with oxygen-enriched room air. Supplemental doses were injected as necessary (0.5 ml/kg) to maintain an appropriate level of anesthesia. Body temperature was maintained at ~38°C with a heating pad. AP was measured by using a high-fidelity pressure transducer (SPC-330A, Millar Instruments, Houston, TX) inserted via the left femoral artery. To record cardiac SNA, we exposed the left cardiac sympathetic nerve through a midline thoracotomy and attached a pair of stainless steel wire electrodes (Bioflex wire AS633, Cooner Wire, Chatsworth, CA) to the nerve. The nerve fibers peripheral to the

Address for reprint requests and other correspondence: D. Michikami, Dept. of Cardiovascular Dynamics, Advanced Medical Engineering Center, National Cardiovascular Center Research Institute, 5-7-1 Fujishirodai, Suita, Osaka 565-8565, Japan (e-mail: dmichi@ri.ncvc.go.jp or kamiya@ri.ncvc.go.jp).

The costs of publication of this article were defrayed in part by the payment of page charges. The article must therefore be hereby marked "*advertisement*" in accordance with 18 U.S.C. Section 1734 solely to indicate this fact.

electrodes were sectioned to eliminate afferent signals from the heart. To insulate and fix the electrodes, the nerves and electrodes were secured with silicone glue (Kwik-Sil, World Precision Instruments, Sarasota, FL). The preamplified nerve signals were band-pass filtered at 150–1,000 Hz, full-wave rectified, and low-pass filtered at a cutoff frequency of 30 Hz by using analog circuit. After that, the neural signals were recorded at a sampling rate of 200 Hz using a 12-bit analog-to-digital converter. Pancuronium bromide (0.1 mg/kg) was administered to prevent contaminating muscular activities. At the end of the experiment, the experimental animals were killed by an overdose of intravenous pentobarbital sodium, and the background noise level of SNA was determined postmortem.

Sixteen of the 22 rabbits were used in *protocol 1 (protocols 1-1, 1-2, and 1-3)*, and the remaining 6 rabbits were used in *protocols 2, 3,* and *4*. In 10 of the 16 rabbits for *protocols 1-2* and/or *1-3* described below, we isolated both carotid sinuses from the systemic circulation by ligating the internal and external carotid arteries and other small branches originating from the carotid sinus regions. The isolated carotid sinuses were filled with warmed physiological saline through catheters inserted via the common carotid arteries. The intra-carotid sinus pressure (CSP) was controlled by a servo-controlled piston pump (model ET-126A, Labworks, Costa Mesa, CA). In the baroreflex open-loop experimental settings, bilateral vagal and aortic depressor nerves were sectioned at the neck to minimize reflex effects from cardiopulmonary regions and the aortic arch.

Electroacupuncture

Two stainless steel needles were inserted at the one-fifth point (from the knee) and the midpoint of the knee-ankle distance of approximately 30–35 mm. These needles with a diameter of 0.2 mm (CE0123, Seirin-Kasei, Shimizu City, Japan) were inserted to a depth of ~10 mm in the skin and underlying muscle (the right tibialis anterior muscle). This area corresponds to the Zusanli and Xiajuxu acupoints (over the peroneal nerve below the knee, stomach meridian, St 36 and 39) in humans.

As in previous studies (2, 3, 17, 42), the stimulus current intensity was determined as 10 times of twitch threshold, which is the minimal electrical current required for eliciting visible muscle twitches of the stimulated leg. Actually, the current was 4.8 ± 0.3 mA (4.2–5.4 mA). An electric rectangular wave current with a frequency of 1 Hz and with pulse duration of 5 ms was passed between these two needles by using an electrical stimulator (SEN-7203, Nihon Kohden) except *protocol 4* where shorter pulse durations were challenged.

Protocols

The experimental protocol was approved by the Animal Experimental Committee of National Cardiovascular Center Research Institute.

Protocol 1: effect of Zusanli electroacupuncture on AP, SNA, and baroreflex. PROTOCOL 1-1 (BAROREFLEX CLOSED-LOOP CONDITION, N = 6). To elucidate the overall cardiovascular inhibitory effects of electroacupuncture, we performed 1 Hz electroacupuncture for 8 min and measured AP and SNA responses under conditions of intact cardiovascular reflexes. In this closed-loop protocol, vagal and aortic depressor nerves were preserved. Baseline data were measured for 1 min before acupuncture insertion. At 10 min after acupuncture insertion, baseline data were measured again for 1 min. Electroacupuncture was applied for 8 min. The recovery data were measured for 2 min after the cessation of electroacupuncture.

PROTOCOL 1-2 (BAROREFLEX OPEN-LOOP CONDITION, N = 8). To elucidate the effects of electroacupuncture on the arterial baroreflex over an entire operating range, we performed a baroreflex open-loop experiment as follows. CSP was first decreased to 40 mmHg. After attainment of a steady state, CSP was increased from 40 to 160 mmHg in increments of 20 mmHg. Each pressure step was maintained for 60 s. We measured AP and SNA during the stepwise increase in CSP. Two trials (control and electroacupuncture trials) were performed on each rabbit. The order of the trials was randomized. The electroacupuncture trial was identical to the control trial except that electroacupuncture was commenced 1 min before the initiation of stepwise increase in CSP.

PROTOCOL 1-3 (BAROREFLEX OPEN-LOOP CONDITION WITH PERONEAL DENERVATION, N = 6). To identify the afferent pathway of electroacupuncture, we examined the effects of 1 Hz electroacupuncture on the arterial baroreflex after severing the right peroneal nerve at the level of the knee joint. Estimation of the baroreflex equilibrium diagram was conducted as in *protocol 1-2* in the control and electroacupuncture trials. Four of the six rabbits had also undergone *protocol 1-2*.

Protocol 2: effects of sham (nonelectrical) acupuncture at Zusanli and control (nonspecific) electrical and nonelectrical acupunctures on AP and SNA in baroreflex closed-loop condition (n = 6). To determine whether changes in AP and SNA during Zusanli electroacupuncture are specific responses, sham and control acupunctures were conducted under the following acupuncture conditions: *1*) no acupuncture (nonacupuncture), *2*) nonelectrical acupuncture at Zusanli-Xiajuxu (St 36–39) acupoints (sham acupuncture), *3*) nonelectrical acupuncture at Guangming-Xuanzhong (gallbladder meridian, Gb 37–39) acupoints (control acupuncture), and *4*) electrical acupuncture at Guangming-Xuanzhong acupoints (control electroacupuncture). We chose Guangming-Xuanzhong as nonspecific control acupoints (*trials 3* and *4*) because these acupoints are believed to reduce leg pain without affecting the cardiovascular system, in contrast to the Zusanli-Xiajuxu acupoints. In each trial, AP and SNA were measured for a baseline duration of 1 min, under acupuncture condition (*trial 1, 2, 3,* or *4*) for 8 min, and recovery for 1 min.

Protocol 3: effect of long-term Zusanli electroacupuncture on AP and SNA in baroreflex closed-loop condition (n = 6). To clarify the effect of long-term electroacupuncture on cardiovascular system, AP and SNA were measured during and after 30 min of electroacupuncture at Zusanli-Xiajuxu acupoints. *Protocol 3* was conducted in the same manner as *protocol 1-1* except with a longer stimulation duration than *protocol 1-1* (8 min).

Protocol 4: Effect of pulse duration of Zusanli electroacupuncture on AP and SNA in baroreflex closed-loop condition (n = 6). To examine the effect of pulse duration of electroacupuncture on AP and SNA, AP and SNA were measured during electroacupuncture at Zusanli-Xiajuxu acupoints with the pulse duration increasing stepwise from 0.1 to 0.25, 0.5, 1, 2.5, 5, and 10 ms, every 60 s. In each animal, the frequency and stimulus current intensity were maintained constant as in *protocols 1, 2,* and *3*.

Data Analysis

We recorded CSP, SNA, and AP at a sampling rate of 200 Hz by using a 12-bit analog-to-digital converter. Data were stored on the hard drive of a dedicated laboratory computer system for later analyses.

In *protocol 1-1, 2, and 4*, mean AP and SNA for 1 min were calculated for baseline conditions, every minute of electroacupuncture, and recovery. In *protocol 3*, mean AP and SNA for 5 min were calculated for baseline conditions, electroacupuncture, and recovery. In *protocols 1-2* and *1-3*, we calculated mean AP and SNA during the last 10 s of each CSP step. Because the absolute magnitude of SNA depended on recording conditions, SNA was presented in arbitrary units (au). The background noise level was set at 0 au and the SNA value at the closed-loop operating point in the control trial (without electroacupuncture) was set at 100 au for each animal.

A four-parameter logistic function analysis was performed on the neural arc (CSP-SNA data pairs) and the peripheral arc (SNA-AP data pairs) as follows (11)

$$y = \frac{P_1}{1 + \exp[P_2(x - P_3)]} + P_4 \quad (1)$$

where x and y represent the input and the output, respectively. P_1 denotes the response range (i.e., the difference between the maximum and minimum values of y), P_2 is the coefficient of gain, P_3 is the midpoint of the logistic function on the input axis, and P_4 is the minimum value of y. The maximum gain (G_{max}) is calculated from $-P_1P_2/4$ at $x = P_3$. The parameter values were calculated by an iterative nonlinear least-squares regression known as the downhill simplex method.

Statistical Analysis

All data are presented as means ± SD. Differences were considered to be significant when $P < 0.05$. In *protocols 1-1, 2, 3,* and *4*, the effects of electroacupuncture on AP and SNA at different time intervals were evaluated by one-way ANOVA. The Dunnett's test was used for multiple comparisons. In *protocols 1-2* and *1-3*, the effects of electroacupuncture on the four parameters of the logistic functions relating to the neural and peripheral arcs, as well as on the closed-loop operating point, were examined by using a paired *t*-test.

RESULTS

Figure 1*A* (*protocol 1-1*) shows a typical time series of AP and SNA in response to Zusanli-Xiajuxu electroacupuncture with intact cardiovascular reflexes. AP and SNA were reduced immediately after beginning electroacupuncture, and these remained reduced during 8-min electroacupuncture. Figure 1*B* illustrates the group-averaged AP and SNA in response to electroacupuncture. AP and SNA for baseline were unchanged by acupuncture insertion alone, while these values for 8-min electroacupuncture remained decreased from baseline. These values returned to baseline level after the cessation of electroacupuncture.

Figure 2 (*protocol 1-2*) shows a typical AP and SNA response to the increments in CSP in the control (Fig. 2, *left*) and electroacupuncture (Fig. 2, *right*) trials. A stepwise increase in CSP decreased SNA and AP in both trials. In the electroacupuncture trial, the AP and SNA response ranges to CSP were attenuated compared with the control trial.

Figure 3, *A* and *B* (*protocol 1-2*), shows the averaged baroreflex neural and peripheral arcs obtained in control and electroacupuncture trials. The neural arc showed a sigmoidal relationship between CSP and SNA. In the neural arc, the response range of SNA (P_1) and midpoint of the operating range (P_3) were significantly decreased by electroacupuncture (Table 1). The coefficient of gain (P_2), the minimum value of SNA (P_4), and G_{max} did not differ between the two trials (Table 1). As a result, the maximum value of SNA, calculated from $P_1 + P_4$, was significantly decreased by electroacupuncture from 162 ± 31 to 130 ± 29 au ($P < 0.005$). The peripheral arc showed a more linear relationship between SNA and AP than the neural arc. In the peripheral arc, electroacupuncture did not affect any of the four parameters or G_{max} (Table 1 and Fig. 3*B*). The operating point determined by the intersection of the neural and peripheral arcs was moved toward lower AP and SNA (from *point a* to *point b*) by electroacupuncture (Fig. 3*C* and Table 1).

Figure 4 (*protocol 1-3*) shows the averaged baroreflex neural (Fig. 4*A*) and peripheral arcs (Fig. 4*B*) in control and electroacupuncture trials with severance of the peroneal nerve innervating the tibialis anterior muscle. Two arcs obtained in both trials were nearly superimposable. The four parameters and G_{max} in the neural and peripheral arcs and operating point were

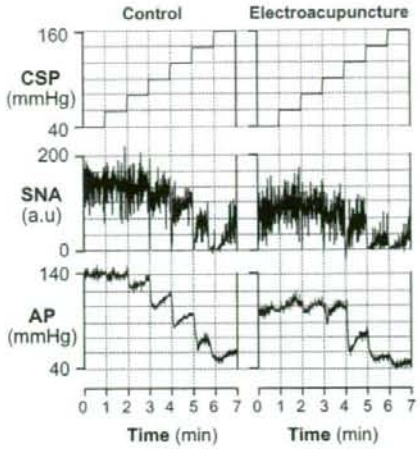

Fig. 2. Typical time series of intra-carotid sinus pressure (CSP), AP, and SNA in control (*left*) and electroacupuncture trials (*right*) in *protocol 1-2*. SNA and AP decreased in response to increments in CSP in both of the two trials. The response ranges of AP and SNA to CSP were lower in electroacupuncture than in controls.

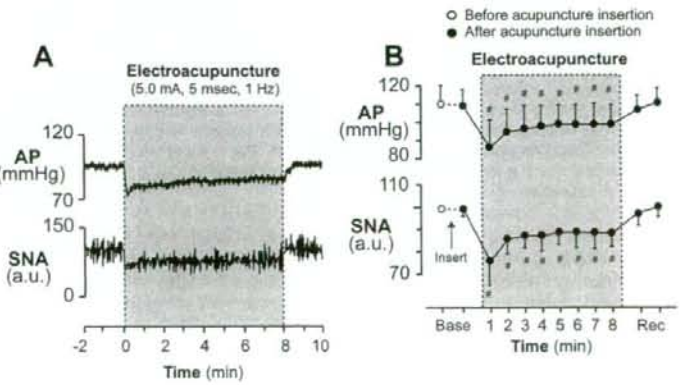

Fig. 1. Typical time series of arterial pressure (AP) and sympathetic nerve activity (SNA) during 8 min of 1-Hz electroacupuncture (*A*) and the averaged ($n = 6$) AP and SNA (*B*) in *protocol 1-1*. Data include periods of baseline (Base, 1 min), electroacupuncture (8 min), and recovery (Rec, 1 min). Each data point represents average values over 1 min. #$P < 0.05$: significantly different from baseline after acupuncture insertion. au, Arbitrary units.

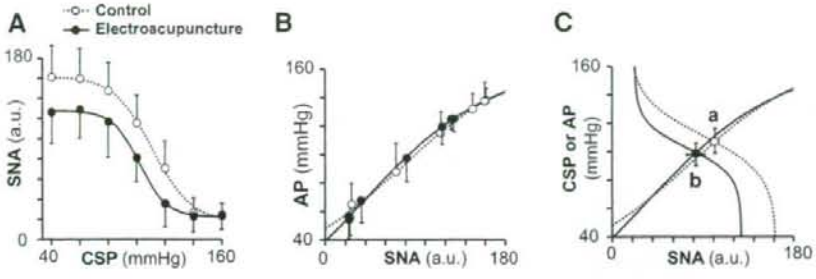

Fig. 3. Averaged (n = 8) baroreflex neural arc (A), peripheral arc (B), and baroreflex equilibrium diagram (C) obtained in 8 rabbits in control (○) and electroacupuncture (●) trials in *protocol 1-2*. Electroacupuncture shifted the neural arc to lower SNA (A), but it did not change the peripheral arc (B). The shift in neural arc reduced AP and SNA by 9 ± 3 mmHg and 20 ± 10 au (from *point a* to *point b*) at the operating point (C).

not affected by electroacupuncture when the peroneal nerve was denervated (Table 2 and Fig. 4*C*).

Figure 5 (*protocol 2*) shows the changes in AP and SNA during nonacupuncture (without acupuncture), sham acupuncture [nonelectrical acupuncture at Zusanli-Xiajuxu (St 36–39)], control acupuncture [nonelectrical acupuncture at Guangming-Xuanzhong (Gb 37–39)] and control electroacupuncture (electrical acupuncture at Gb 37–39) trials. AP and SNA did not change in these trials.

Figure 6, *A* and *B* (*protocol 3*), shows a typical time series and the averaged data, respectively, of AP and SNA in response to long-term Zusanli-Xiajuxu electroacupuncture. AP and SNA decreased immediately after electroacupuncture was started and remained reduced during 30-min electroacupuncture. In addition, AP and SNA returned to the preelectroacupuncture baseline levels immediately after cessation of electroacupuncture.

Figure 7, *A* and *B* (*protocol 4*), shows a typical time series and the averaged data, respectively, of AP and SNA during Zusanli-Xiajuxu electroacupuncture with the pulse duration increasing from 0.1 to 5 ms. Although increasing the pulse duration from 0.1 to 1 ms did not change AP and SNA, pulse durations of 2.5 ms and higher decreased SNA while pulse durations of 5 and 10 ms decreased AP.

Table 1. *Effect of electroacupuncture on the operating point of baroreflex and on the 4 parameters of logistic functions approximating neural and peripheral baroreflex arcs*

	Control	Electroacupuncture
Operating point		
Arterial pressure, mmHg	108.4±8.7	98.8±7.9†
Sympathetic nerve activity, au	99.8±4.1	80.0±8.9†
Neural arc		
P_1, au	144.0±35.0	112.6±9.2†
P_2, au/mmHg	0.08±0.03	0.09±0.09
P_3, mmHg	111.4±6.5	103.3±10.0*
P_4, au	17.5±6.1	17.4±8.7
G_{max}, au/mmHg	−2.94±0.91	−2.58±1.27
Peripheral arc		
P_1, mmHg	129.6±20.5	125.9±19.5
P_2, au/mmHg	−0.03±0.01	−0.03±0.01
P_3, au	80.6±23.2	71.7±17.1
P_4, mmHg	29.9±16.3	29.5±12.1
G_{max}, mmHg/au	0.74±0.10	0.84±0.18

Values are means ± SD (n = 8). G_{max}, maximum gain. See *Data Analysis* for definition of 4 parameters of logistic function. au, Arbitrary units. *P < 0.05 and †P < 0.005 vs. control.

DISCUSSION

The major new finding of the present study was that electroacupuncture at Zusanli resets the arterial baroreflex neural arc to lower SNA but does not significantly affect the baroreflex peripheral arc. As a result, the operating point determined by the intersection of the neural and peripheral arcs was moved toward lower SNA and AP by electroacupuncture. To the best of our knowledge, this is the first study delineating the effects of short-term electroacupuncture on the arterial baroreflex over an entire operating range.

Effects of Electroacupuncture on the Arterial Baroreflex (Protocol 1)

The arterial baroreflex system is one of the most important negative-feedback systems that stabilize AP against exogenous disturbances. When AP is decreased by exogenous perturbation such as blood loss, the reduction in AP is sensed by the arterial baroreceptors. SNA is then increased by the arterial baroreflex to buffer the reduction in AP. In such circumstances, SNA and AP change reciprocally. On the other hand, when SNA is changed by an exogenous perturbation such as emotional stress, SNA and AP change in parallel. In *protocol 1-1*, electroacupuncture decreased both SNA and AP, indicating that electroacupuncture introduced exogenous perturbation to decrease SNA with a resultant reduction in AP. Although the net effect of electroacupuncture is to decrease SNA, the perturbation of AP cannot be excluded. For example, because electroacupuncture also twitched the hindlimb muscles, electroacupuncture might have perturbed AP via changes in vascular resistance and/or venous return through muscle pump function. Therefore, to quantify the contribution of both perturbations on SNA and on AP, we performed *protocol 1-2*. Perturbation of AP is most easily detected by comparing AP at the same SNA level with and without electroacupuncture.

In *protocol 1-2*, we performed a baroreflex open-loop experiment and identified the static characteristics of the neural and peripheral arcs over a wide operating range. As expected, electroacupuncture shifted the neural arc toward lower SNA and decreased maximum SNA to ~80% of control (Fig. 3*A*). This shift is not due to reduced perfusion to the medulla by AP reduction during electroacupuncture because the AP was decreased by ~10 mmHg and would not induce cerebral ischemia. In contrast, electroacupuncture had little effect on the peripheral arc (Fig. 3*B*). In other words, AP with and without electroacupuncture did not differ significantly at any of the SNA levels. Therefore, changes in AP observed in *protocol 1-1*

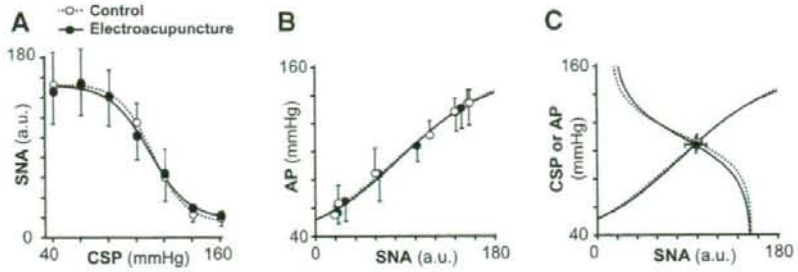

Fig. 4. Averaged (n = 6) baroreflex neural arc (A), peripheral arc (B), and baroreflex equilibrium diagrams (C) obtained in 6 rabbits in control (○) and electroacupuncture (●) trials with peroneal denervation in *protocol 1-3*. The baroreflex neural arc, peripheral arc, and the operating point were not influenced by electroacupuncture after peroneal denervation.

were attributable exclusively to perturbation of SNA and not to possible perturbation effects of electroacupuncture on AP.

The neural and peripheral arcs were combined to yield a baroreflex equilibrium diagram (Fig. 3*C*). The closed-loop operating point, determined by the intersection of the neural and peripheral arcs, moved from *point a* to *point b* during electroacupuncture. Despite a significant shift in the closed-loop operating point, neither the neural nor peripheral arc gain was altered significantly (Table 1). The fact that the baroreflex gain was maintained during electroacupuncture suggests the possible application of electroacupuncture to the treatment of cardiovascular diseases with sympathetic hyperactivity. However, the preservation of the arterial baroreflex gain in the present experimental settings may rely on normal peripheral arc characteristics. Cardiovascular diseases such as heart failure may decrease the peripheral arc gain to a variable extent due to impaired pump function. Whether the arterial baroreflex function during electroacupuncture can be maintained in cardiovascular diseases awaits future study.

Mechanisms for the Cardiovascular Inhibitory Effects of Electroacupuncture (Protocol 1)

The resetting in the baroreflex neural arc during electroacupuncture was mediated by a somatosympathetic reflex arising from the stimulated hindlimb, as evidenced by the fact that peroneal denervation abolished the resetting (Table 2 and Fig. 4). This result was consistent with an earlier study (27) showing that depressor and sympathoinhibitory responses during acupuncture were abolished by sciatic and femoral denervation. The existence of a somatosympathetic reflex is also supported by the fact that electrical stimulation of somatic afferents reduced AP (7–9). Legramante et al. (14) showed that rapidly conducting group III somatic afferent activation can evoke AP reduction during 1-Hz electrical stimulation of the tibial nerve. In contrast, high-frequency stimulation of the somatic afferent evokes AP elevation. Passive muscle stretching, which is considered to activate group III somatic afferent fibers, shifts the baroreflex neural arc toward higher SNA, resulting in an increase in the closed-loop operating point (41). The mechanism of two opposing influences of somatic afferent activation depending on the stimulation frequency is not fully understood.

Table 2. *Effect of electroacupuncture with peroneal denervation on the operating point of baroreflex and on the 4 parameters of logistic functions approximating neural and peripheral baroreflex arcs*

	Control	Electroacupuncture
Operating point		
Arterial pressure, mmHg	105.7±5.7	104.1±5.6
Sympathetic nerve activity, au	99.8±5.1	98.3±11.1
Neural arc		
P_1, au	138.3±42.4	136.3±38.6
P_2, au/mmHg	0.11±0.03	0.08±0.03
P_3, mmHg	112.7±10.2	111.5±10.6
P_4, au	14.9±8.7	15.7±7.4
G_{max}, au/mmHg	−3.27±1.15	−2.84±1.12
Peripheral arc		
P_1, mmHg	144.1±35.5	140.5±34.4
P_2, au/mmHg	−0.02±0.002	−0.02±0.004
P_3, au	82.0±34.0	78.8±32.0
P_4, mmHg	26.1±8.1	25.5±5.3
G_{max}, mmHg/au	0.69±0.13	0.72±0.21

Values are means ± SD (n = 6). See *Data Analysis* for definition of 4 parameters of logistic function.

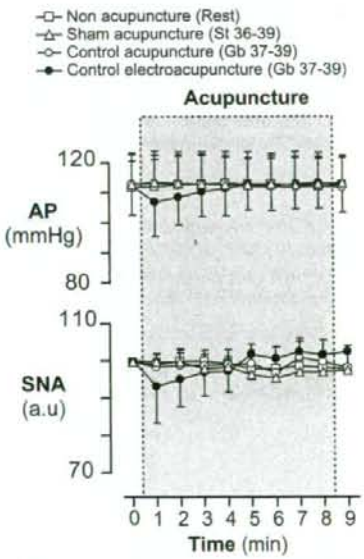

Fig. 5. Averaged (n = 6) AP (*top*) and SNA (*bottom*) in nonacupuncture (condition without acupuncture, □), sham acupuncture [nonelectrical acupuncture at Zusanli-Xiajuxu (stomach meridian, St 36–39), △], control acupuncture [nonelectrical and acupuncture at Guangming-Xuanzhong (gallbladder meridien, Gb 37–39), ○], and control electroacupuncture [electrical acupuncture at Gb 37–39, ●] trials in *protocol 2*. Data include periods of baseline (1 min), electroacupuncture (8 min), and recovery (1 min). Each data point represents average values over 1 min.

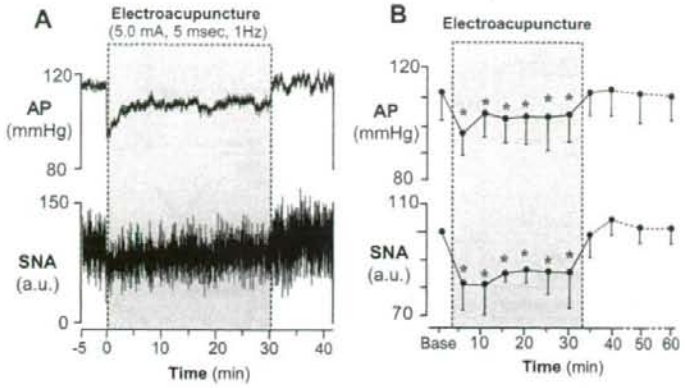

Fig. 6. Typical time series of AP and SNA during 30 min of 1-Hz electroacupuncture (St 36–39; *A*) and the averaged (n = 6) AP and SNA (*B*) in *protocol 3*. Data include periods of baseline (5 min), electroacupuncture (30 min), and recovery (30 min). Each data point represents averaged values over 5 min during baseline, electroacupuncture, and the first 10 min of recovery and those over 10 min during the last 20 min of recovery. *$P < 0.05$: significantly different from baseline after acupuncture insertion.

Another explanation for resetting in the neural arc may be circulatory endogenous opioids (e.g., β-endorphin and enkephalin), which are released from the adrenal gland and hypothalamus by prolonged (>30 min) electroacupuncture (20, 21). These endogenous opioids are known to modulate the arterial baroreflex (24, 29, 35). However, changes in endogenous opioids are unlikely to be the mechanism for reductions in SNA and AP by electroacupuncture in the present experimental settings because the inhibitory effects terminated immediately after cessation of electroacupuncture rather than lasting for several hours (42) (Fig. 1).

Previous studies suggest a central interaction between an electroacupuncture-evoked somatosympathetic reflex and the arterial baroreflex. Baroreceptor afferent inputs inhibit neural activities in the rostral ventrolateral medulla (rVLM) (6, 33). Tjen-A-Looi et al. (36) showed that electroacupuncture inhibited rVLM neural activities, suggesting that the electroacupuncture-evoked somatosympathetic reflex and arterial baroreflex share common central pathways. In addition, 2-Hz electroacupuncture inhibits SNA through the excitation of β-endorphinergic and GABAergic neurons to rVLM (12, 13).

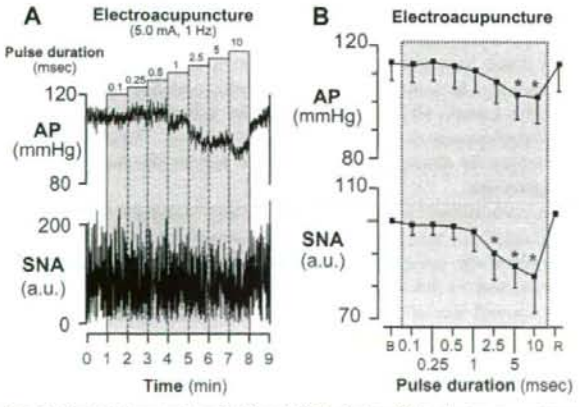

Fig. 7. Typical time series of AP and SNA during 1-Hz electroacupuncture with increasing the pulse duration (*A*) and the averaged (n = 6) AP and SNA (*B*) in *protocol 4*. Data include periods of baseline (B, 1 min), electroacupuncture (7 min), and recovery (R, 1 min). Each data point represents average values over 1 min. *$P < 0.05$; significantly different from baseline after acupuncture insertion.

Central interaction in the brain stem may be involved in the resetting of the arterial baroreflex neural arc induced by electroacupuncture.

Characteristics of Zusanli-Xiajuxu Electroacupuncture Used in the Present Study

The Zusanli electroacupuncture used in this study has some unique characteristics. First, our results showed that baseline AP and SNA were decreased significantly by electroacupuncture, in contrast to previous studies that found no significant reduction in baseline AP and SNA during Zusanli electroacupuncture in rats (0.5-ms duration, 1–2 mA, 2 Hz) (18) and nonelectrical acupuncture in normotensive humans (right large intestine 4, right liver 3, and left spleen 6) (22). Second, our result showed that AP and SNA were reduced as soon as electroacupuncture was started, in contrast to previous reports that the effect of Zusanli electroacupuncture did not even begin to manifest for the first 10–15 min in rats (0.5-ms duration, 1–2 mA, 2 Hz) (18) and cats (0.5-ms duration, 0.4–0.6 mA, 2–4 Hz) (37). These discrepancies may be related to the differences in acupoints and stimulation conditions (pulse duration, current, and frequency). In particular, the pulse duration used in our study (5 ms) was approximately 10–50 times longer than that used in previous studies. Indeed, the data obtained from *protocol 4* show that increasing the pulse duration augments the reduction in AP and SNA during electroacupuncture; pulse durations shorter than 2.5 ms did not change AP and SNA, whereas durations of 2.5 ms and above decreased both parameters immediately after the electroacupuncture was started (Fig. 7). In addition, our data suggest that stimulation duration (<2.5 ms) does not affect arterial baroreflex, consistent with our preliminary data that baroreflex neural, peripheral, and total arcs remained unchanged during electroacupuncture with pulse durations <2.5 ms (unpublished data). These observations may indicate that the effect of electroacupuncture on arterial baroreflex is linked to the stimulation pulse duration.

The third characteristic is that the inhibitory effects of electroacupuncture on AP and SNA disappeared immediately after the cessation of electroacupuncture. In contrast, some studies showed that the inhibitory effects of electroacupuncture on AP lasted for 10–60 min after the cessation (18). The characteristics in this study may not be explained by the length of electroacupuncture because AP and SNA recovered to the

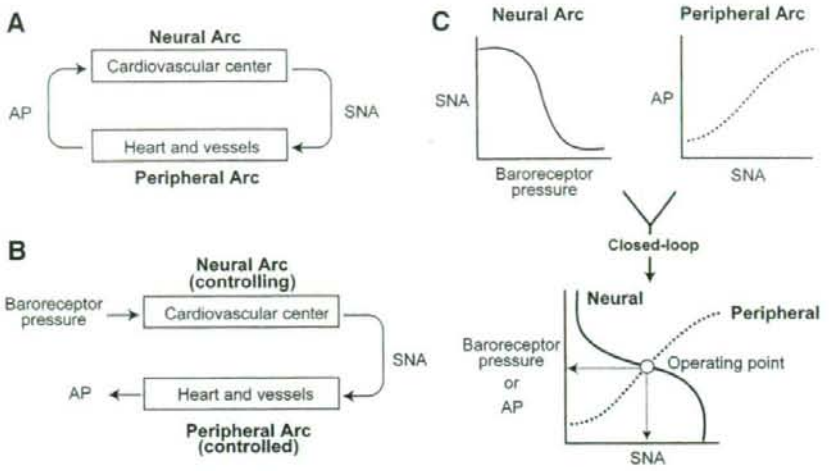

Fig. 8. Arterial baroreflex system in closed-loop (*A*) and open-loop (*B*) conditions. In open-loop conditions, the relationships between baroreceptor pressure and SNA (the neural arc) and between SNA and AP (the peripheral arc) can be quantitatively measured. Intersection of the neural and peripheral arcs corresponds to the operating point of AP and SNA under closed-loop conditions of feedback (*C*).

prestimulation baseline levels immediately after the cessation in both short-duration (8 min, Fig. 1) and longer-duration electroacupuncture (30 min, Fig. 6) protocols. The rapid disappearance of effects suggests that the AP and SNA reductions seen in the present study may not be elicited by the opioid mechanism, although clinical experiments with longer-duration electroacupuncture have demonstrated long-lasting effects on the cardiovascular system, which are attributed to opioid substances (2, 12, 15, 37, 42).

The reductions in AP and SNA during Zusanli electroacupuncture seen in the present study may not be just a nonspecific response to acupunctures. Our data from *protocol 2* (Fig. 5) showed that nonelectrical acupuncture at Zusanli (sham acupuncture) did not decrease AP and SNA, suggesting that the AP and SNA reductions during Zusanli electroacupuncture are not simply the results from insertion of acupuncture needles. Furthermore, acupuncture at Guangming-Xuanzhong (control acupuncture, control electroacupuncture) did not change AP and SNA regardless of electrical stimulation (Fig. 5). This result suggests the importance of acupoint specificity and is consistent with an earlier study showing point-specific differences in cardiovascular inhibitory responses (Jiangshi-Neiguan or Shousanli-Quchi acupoints vs. Pianli-Wenlui or Zusanli-Shangjuxu acupoints) (37). These observations may support the concept that Zusanli acupuncture changes cardiovascular variables in experimental animal models (4, 25, 28) and confers beneficial effects on cardiovascular diseases (5, 30, 34), whereas Guangming-Xuanzhong acupuncture does not affect cardiovascular variables (18).

Limitations

There are several limitations to this study. First, as anesthesia affects the autonomic nervous system, the results might have been different without anesthesia. Second, our isolation of the carotid sinus regions may stimulate carotid chemoreceptors. However, in determining baroreflex function, this factor was present in trials with and without electroacupuncture. Therefore, we believe that this factor may not affect our conclusion of baroreflex resetting during electroacupuncture.

Third, acupuncture was inserted at a point corresponding to the Zusanli acupoint in humans. When acupuncture is properly inserted at the acupoint, the patient feels heaviness or soreness. Such sensory information is not available in an anesthetized animal. Because electroacupuncture (as distinct from acupuncture with no electrical stimulation) stimulates not only the inserted point but also the surrounding area, it has been used as a convenient way of stimulating acupoints in patients and in experimental animals. Thus, even if we failed to insert the needle at the precise acupoint, we believe that Zusanli could be stimulated electrically.

Fourth, although we determined the effects of electroacupuncture at Zusanli acupoints on cardiovascular and baroreflex systems, there are other important acupoints that are able to influence these systems. In particular, Neiguan electroacupuncture is actually known to decrease sympathetic premotor neuron activity for a longer period than Zusanli electroacupuncture (36, 37). Further studies are necessary to determine the effect of Neiguan electroacupuncture on the arterial baroreflex.

Last, we evaluated the effects of Zusanli electroacupuncture on the baroreflex function for a short acupuncture duration of only 8 min. Because electroacupuncture is typically practiced for longer periods of time, our results have limited applicability. However, the electroacupuncture we used decreased AP and SNA immediately after application, showing that the procedure has acute effect on the cardiovascular system. That was the reason why we focused on the effect of short duration electroacupuncture on the baroreflex system. Future study is necessary to examine the effects of longer-duration electroacupuncture.

In conclusion, 1 Hz, short-term electroacupuncture of Zusanli reset the baroreflex neural arc toward lower SNA but did not affect the peripheral arc. The closed-loop operating point determined by the intersection of the neural and peripheral arcs was moved toward lower SNA and AP by electroacupuncture.

APPENDIX

Theoretical Considerations: Coupling of Neural and Peripheral Arcs

Changes in AP are immediately sensed by arterial baroreceptors, which alter efferent SNA via the cardiovascular center of baroreflex (Fig. 8*A*). Efferent SNA in turn governs heart rate and the mechanical

properties of the heart and vessels, which themselves exert a direct influence over AP. This negative-feedback loop makes it difficult to analyze the behavior of the arterial baroreflex. To overcome this problem, we opened the negative-feedback loop and divided the system into controlling and controlled elements (31). We defined the controlling element as the neural arc and the controlled element as the peripheral arc (Fig. 8*B*). In the neural arc, the input is the pressure sensed by the arterial baroreceptors and the output is SNA. In the peripheral arc, the input is SNA and the output is AP (Fig. 8*C*). Because pressure sensed by the arterial baroreceptor is equilibrated with AP under physiological conditions, we superimposed the functions of the two arcs and determined the operating point of the system from the intersection of the two arcs. The operating point is defined as the AP and SNA under closed-loop conditions of the feedback system. The validity of this framework has been examined in previous studies (10, 31). Using the baroreflex equilibrium diagram, we aimed to quantify the effects of electroacupuncture on the arterial baroreflex.

GRANTS

This study was supported by Health and Labor Sciences Research Grant for Research on Advanced Medical Technology from the Ministry of Health, Labour, and Welfare of Japan (H14-Nano-002), by a Grant-in-Aid for Scientific Research (A) (15200040) from the Japan Society for the Promotion of Science, the Program for Promotion of Fundamental Studies in Health Science from the Pharmaceutical and Medical Devices Agency of Japan, and by the "Ground-based Research Announcement for Space Utilization" project promoted by Japan Space Forum. This study was also supported by Industrial Technology Research Grant Program in 03A47075 from New Energy and Industrial Technology Development Organization (NEDO) of Japan.

REFERENCES

1. **Brickman AL, Calaresu FR, and Mogenson GJ.** Bradycardia during stimulation of the septum and somatic afferents in the rabbit. *Am J Physiol Regul Integr Comp Physiol* 236: R225–R230, 1979.
2. **Chao DM, Shen LL, Tjen-A-Looi S, Pitsillides KF, Li P, and Longhurst JC.** Naloxone reverses inhibitory effect of electroacupuncture on sympathetic cardiovascular reflex responses. *Am J Physiol Heart Circ Physiol* 276: H2127–H2134, 1999.
3. **Chen S and Ma SX.** Nitric oxide in the gracile nucleus mediates depressor response to acupuncture (ST36). *J Neurophysiol* 90: 780–785, 2003.
4. **Chiu DTJ and Cheng KK.** A study of the mechanism of the hypotensive effect of acupuncture in the rat. *Am J Chin Med* 2: 413–419, 1974.
5. **Chiu YJ, Chi A, and Reid IA.** Cardiovascular and endocrine effects of acupuncture in hypertensive patients. *Clin Exp Hypertens* 19: 1047–1063, 1997.
6. **Dampney RA, Horiuchi J, Tagawa T, Fontes MA, Potts PD, and Polson JW.** Medullary and supramedullary mechanisms regulating sympathetic vasomotor tone. *Acta Physiol Scand* 177: 209–218, 2003.
7. **Johansson B.** Studies on cardiovascular responses induced by electrical stimulation of afferent somatic nerves. A preliminary report. *Med Exp Int J Exp Med* 5: 447–453, 1961.
8. **Johansson B.** Circulatory responses to stimulation of somatic afferents with special reference to depressor effects from muscle nerves. *Acta Physiol Scand Suppl* 198: 1–91, 1962.
9. **Johansson B, Lundgren O, and Mellander S.** Reflex influence of "somatic pressor and depressor afferents" on resistance and capacitance vessels and on transcapillary fluid exchange. *Acta Physiol Scand* 62: 280–286, 1964.
10. **Kawada T, Shishido T, Inagaki M, Zheng C, Yanagiya Y, Uemura K, Sugimachi M, and Sunagawa K.** Estimation of baroreflex gain using a baroreflex equilibrium diagram. *Jpn J Physiol* 52: 21–29, 2002.
11. **Kent BB, Drane JW, Blumenstein B, and Manning JW.** A mathematical model to assess changes in the baroreceptor reflex. *Cardiology* 57: 295–310, 1972.
12. **Ku YH and Chang YZ.** β-Endorphin- and GABA-mediated depressor effect of specific electroacupuncture surpasses pressor response of emotional circuit. *Peptides* 22: 1465–1470, 2001.
13. **Ku YH and Zou CJ.** Beta-endorphinergic neurons in nucleus arcuatus and nucleus tractus solitarii mediated depressor-bradycardia effect of "Tinggong" 2-Hz electroacupuncture. *Acupunct Electrother Res* 18: 175–184, 1993.
14. **Legramante JM, Raimondi G, Adreani CM, Sacco S, Iellamo F, Peruzzi G, and Kaufman MP.** Group III muscle afferents evoke reflex depressor responses to repetitive muscle contractions in rabbits. *Am J Physiol Heart Circ Physiol* 278: H871–H877, 2000.
15. **Li L, Yin-Xiang C, Hong X, Peng L, and Da-Nian Z.** Nitric oxide in vPAG mediates the depressor response to acupuncture in stress-induced hypertensive rats. *Acupunct Electrother Res* 26: 165–170, 2001.
16. **Li P.** The effect of acupuncture on blood pressure: the interrelation of sympathetic activity and endogenous opeoid peptides. *Acupunct Electrother Res* 8: 45–56, 1983.
17. **Li P, Pitsillides KF, Rendig SV, Pan HL, and Longhurst JC.** Reversal of reflex-induced myocardial ischemia by median nerve stimulation: a feline model of electroacupuncture. *Circulation* 97: 1186–1194, 1998.
18. **Li P, Rowshan K, Crisostomo M, Tjen-A-Looi SC, and Longhurst JC.** Effect of electroacupuncture on pressor reflex during gastric distension. *Am J Physiol Regul Integr Comp Physiol* 283: R1335–R1345, 2002.
19. **Li P, Tjen-A-Looi S, and Longhurst JC.** Rostral ventrolateral medullary opioid receptor subtypes in the inhibitory effect of electroacupuncture on reflex autonomic response in cats. *Auton Neurosci* 89: 38–47, 2001.
20. **Lin JG, Chang SL, and Cheng JT.** Release of beta-endorphin from adrenal gland to lower plasma glucose by the electroacupuncture at Zhongwan acupoint in rats. *Neurosci Lett* 326: 17–20, 2002.
21. **Lin JG, Lo MW, Wen YR, Hsieh CL, Tsai SK, and Sun WZ.** The effect of high and low frequency electroacupuncture in pain after lower abdominal surgery. *Pain* 99: 509–514, 2002.
22. **Middlekauff HR, Yu JL, and Hui K.** Acupuncture effects on reflex responses to mental stress in humans. *Am J Physiol Regul Integr Comp Physiol* 280: R1462–R1468, 2001.
23. **Mohrman DE and Heller LJ.** *Cardiovascular Physiology* (4th ed.). New York: McGraw-Hill, 1997, p. 158–230.
24. **Moore PG, Quail AW, Cottee DB, McIlveen SA, and White SW.** Effect of fentanyl on baroreflex control of circumflex coronary conductance. *Clin Exp Pharmacol Physiol* 27: 1028–1033, 2000.
25. **Mori H, Uchida S, Ohsawa H, Noguchi E, Kimura T, and Nishijo K.** Electro-acupuncture stimulation to a hindpaw and a hind leg produces different reflex responses in sympathoadrenal medullary function in anesthetized rats. *J Auton Nerv Syst* 79: 93–98, 2000.
26. **Nishijo K, Mori H, Yosikawa K, and Yazawa K.** Decreased heart rate by acupuncture stimulation in humans via facilitation of cardiac vagal activity and suppression of cardiac sympathetic nerve. *Neurosci Lett* 227: 165–168, 1997.
27. **Ohsawa H, Okada K, Nishijo K, and Sato Y.** Neural mechanism of depressor responses of arterial pressure elicited by acupuncture-like stimulation to a hindlimb in anesthetized rats. *J Auton Nerv Syst* 51: 27–35, 1995.
28. **Ohsawa H, Yamaguchi S, Ishimaru H, Shimura M, and Sato Y.** Neural mechanism of pupillary dilation elicited by electro-acupuncture stimulation in anesthetized rats. *J Auton Nerv Syst* 64: 101–106, 1997.
29. **Petty MA and Reid JL.** The effect of opiates on arterial baroreceptor reflex function in the rabbit. *Naunyn Schmiedebergs Arch Pharmacol* 319: 206–211, 1982.
30. **Richter A, Herlitz J, and Hjalmarson A.** Effect of acupuncture in patients with angina pectoris. *Eur Heart J* 12: 175–178, 1991.
31. **Sato T, Kawada T, Inagaki M, Shishido T, Takaki H, Sugimachi M, and Sunagawa K.** New analytic framework for understanding sympathetic baroreflex control of arterial pressure. *Am J Physiol Heart Circ Physiol* 276: H2251–H2261, 1999.
32. **Si QM, Wu GC, and Cao XD.** Effects of electroacupuncture on acute cerebral infarction. *Acupunct Electrother Res* 23: 117–124, 1998.
33. **Sved AF, Ito S, and Madden CJ.** Baroreflex dependent and independent roles of the caudal ventrolateral medulla in cardiovascular regulation. *Brain Res Bull* 51: 129–133, 2000.
34. **Tam KC and Yiu HH.** The effect of acupuncture on essential hypertension. *Am J Chin Med* 3: 369–375, 1975.
35. **Taneyama C, Goto H, Kohno N, Benson KT, Sasao J, and Arakawa K.** Effects of fentanyl, diazepam, and the combination of both on arterial baroreflex and sympathetic nerve activity in intact and baro-denervated dogs. *Anesth Analg* 77: 44–48, 1993.
36. **Tjen-A-Looi SC, Li P, and Longhurst JC.** Prolonged inhibition of rostral ventral lateral medullary premotor sympathetic neurons by electroacupuncture in cats. *Auton Neurosci* 106: 119–131, 2003.

37. **Tjen-A-Looi SC, Peng L, and Longhurst JC.** Medullary substrate and differential cardiovascular responses during stimulation of specific acupoints. *Am J Physiol Regul Integr Comp Physiol* 287: R852–R862, 2004.
38. **Wang JD, Kuo TB, and Yang CC.** An alternative method to enhance vagal activities and suppress sympathetic activities in humans. *Auton Neurosci* 100: 90–95, 2002.
39. **Wong AM, Leong CP, Su TY, Yu SW, Tsai WC, and Chen CP.** Clinical trial of acupuncture for patients with spinal cord injuries. *Am J Phys Med Rehabil* 82: 21–27, 2003.
40. **Wong AM, Su TY, Tang FT, Cheng PT, and Liaw MY.** Clinical trial of electrical acupuncture on hemiplegic stroke patients. *Am J Phys Med Rehabil* 78: 117–122, 1999.
41. **Yamamoto K, Kawada T, Kamiya A, Takaki H, Miyamoto T, Sugimachi M, and Sunagawa K.** Muscle mechanoreflex induces the pressor response by resetting the arterial baroreflex neural arc. *Am J Physiol Heart Circ Physiol* 286: H1382–H1388, 2004.
42. **Yao T.** Acupuncture and somatic nerve stimulation: mechanism underlying effects on cardiovascular and renal activities. *Scand J Rehabil Med Suppl* 29: 7–18, 1993.